ADA062941

LEVEL I

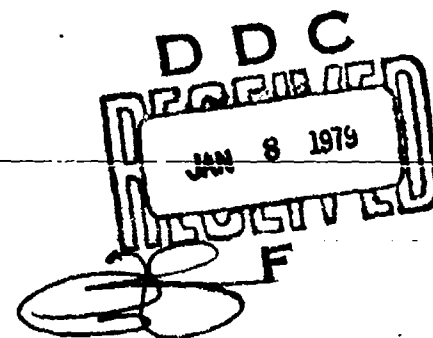EVALUATION OF LIQUID CARGO

TANK OVERPRESSURE

MR. R. SWANEK

DDC

JAN 8 1979

FINAL REPORT

SEPTEMBER 1978

Document is available to the public through the
National Technical Information Service,
Springfield, Virginia 22151

Prepared for

U.S. DEPARTMENT OF TRANSPORTATION
United States Coast Guard
Office of Research and Development
Washington, D.C. 20590

79 01 05 018

NOTICE

Technical Report Documentation Page

1. Report No.	2. Government Accession No.	3. Recipient's Catalog No.
CG-D-71-78		

4. Title and Subtitle		5. Report Date
Evaluation of Liquid Cargo Tank Overpressure		Sep 78
		6. Performing Organization Code

8. Performing Organization Report No.

7. Author's)
Richard Swanek

9. Performing Organization Name and Address	10. Work Unit No. (TRAIS)
Structures Department, Surface Ship Division	3304.01.03.3
David W. Taylor Naval Ship Research & Development Center,	11. Contract or Grant No.
Bethesda, Maryland. 20084	MIPR-Z-70099-6-65865
	13. Type of Report and Period Covered

12. Sponsoring Agency Name and Address	
Department of Transportation	Final Report.
U. S. Coast Guard Hdqtrs.(G-DSA-1/TP44)	
Washington, D. C. 20590	14. Sponsoring Agency Code
	G-DSA-1/TP44

15. Supplementary Notes
84 p.

16. Abstract

The phenomenon of cargo tank overpressure during transfer operations was analyzed and analytical models describing tank pressure rise during transfer operations were validated with scale model experiments. Factors examined affecting tank pressure were cargo properties, transfer rates, tank characteristics and vent system design. Findings indicate that typical vent systems employed today have adequate capacity for venting gas but inadequate capacity to vent liquid after the tank becomes liquid full. Furthermore, it appears that tank failure is inevitable for the case of liquid overfill unless loading rate(cu-ft per sec) to vent area (sq-ft) ratios are kept below 6ft/sec. Currently, most transfer operations exceed this value with tank failure expected less than one minute after the tank becomes liquid full. A method to evaluate the adequacy of existing cargo tanks against the overpressure hazard is presented.

17. Key Words		18. Distribution Statement
Overpressure	Venting	Document is available to the public
Cargo Tank	Vent System	thorugh the National Technical Informa-
Tankers	Vapor Relief	tion Service, Springfield, VA. 22161.
Chemical Tankers	(overfill bulkhead)	

19. Security Classif. (of this report)	20. Security Classif. (of this page)	21. No. of Pages	22. Price
Unclassified	Unclassified	81	

Form DOT F 1700.7 (8-72)   Reproduction of completed page authorized

TABLE OF CONTENTS

i

Page

LIST OF FIGURES

iii

79 0   8

LIST OF TABLES

ABSTRACT

The phenomenon of cargo tank overpressure during transfer operations was analyzed and analytical models describing tank pressure rise during transfer operations validated with scale model experiments. Factors examined affecting tank pressure were cargo properties, transfer rates, tank characteristics and vent system design. Findings indicate that typical vent systems employed today have adequate capacity for venting gas but inadequate capacity to vent liquid after the tank becomes liquid full. Furthermore, it appears that tank failure is inevitable for the case of liquid overfill unless loading rate (cu-ft per sec) to vent area (sq-ft) ratios are kept below 6 ft/sec. Currently, most transfer operations exceed this value with tank failure expected less than one minute after the tank becomes liquid full. A method to evaluate the adequacy of existing cargo tanks against the overpressure hazard is presented.

ADMINISTRATIVE INFORMATION

ACKNOWLEDGEMENTS

vi

I. BACKGROUND AND SUMMARY OF FINDINGS

Background

Venting systems are employed on marine vessels to relieve pressure differences which arise between the cargo tank and the ambient. Various types of venting systems are employed, depending on the cargo being transferred. Typical venting systems can employ the use of flame screens, PV valves and/or flame arresters, as well as other plumbing type fixtures, and may have open or closed gauging. If the cargo transfer rate exceeds the vapor relief capacity, or if an accidental overfilling of the tank occurs, the resulting pressure difference can, depending upon bulkhead structural design, result in tank damage or failure.

An analytical study of the overpressure phenomena has been performed by Arthur D. Little, Inc. (ADL)[1]. The analytical study evaluates the overpressure of any given cargo transfer operation based on cargo properties, transfer rate, tank structural characteristics, and vent system design. It is the intent of the investigation included herein to validate the engineering analysis of the ADL study through the use of scale model experiments and to lend credence to design and operational guidelines to be based on these studies.

Summary of Findings

1. The ADL analytical formulations for the cases of gas venting or liquid overfill during normal loading of cargo were found to be valid for the range of loading rates, evaporation rates, and vent system restrictions examined.

---

[1] References are listed on page 63.

1

2. For normal vent systems, cargo volatilities, and cargo loading rates, it appears that cargo can be loaded with an adequate safety factor so as not to approach the average 6 psig estimated tank failure pressure.[1]

3. An analytical formulation for offloading cargo is developed and validated with scale model experiments.

    a. The absolute value of the magnitude of negative pressure during offloading is less than the absolute value of the magnitude of positive pressure realized when loading cargo for equal values of transfer rate and vent system resistance.

    b. There is a possibility of the tank top buckling inward, especially when the tank top is cambered, at a negative gage pressure which is smaller in absolute magnitude than the 6 psig at which the tank would fail in overpressure.

4. Simplified expressions are developed which can be employed to calculate the maximum positive or negative gage pressure realized for loading or offloading non-volatile cargoes.

5. For high loading rates and/or vent restrictions, the maximum tank top pressure changes rapidly with small changes in loading rate, indicating the danger in employing these higher rates.

6. Evaluation of the pressure buildup during liquid overfill suggests that tank failure is inevitable unless very low ratios of loading rate (ft^3/sec) to vent area (ft^2) are employed. This study found that 6 ft/sec is the maximum permissible ratio (based on a 4fL/D=10 and H=8ft), while ratios of 30 ft/sec and greater are commonly employed.

7. The analytical model for the case of a blocked vent provides an easily employed and conservative estimate of the time it will take to reach the tank failure pressure.

8. Tank flexibility and the inclusion of trapped air in the tank help to reduce the rate of the pressure buildup in the tank during liquid overfill, but not such that the danger presented by liquid overfill is diminished. Furthermore, because of the relatively short time required to reach tank failure (typically less than 30 seconds after the tank becomes liquid full), it appears that the overfill situation must be prevented from occurring.

II. CARGO TRANSFER AND PARAMETERS AFFECTING TANK PRESSURE

A. Cargo Tank and Vent System Configurations

Cargo tanks on chemical tankers and barges are partitioned into indi-vidual tanks for structural and cargo segregation purposes. The tanks, vent systems and pumps are matched to insure efficient loading and off-loading operations. Typically, more than one tank would be loaded simul-taneously, with groups of four being most common.

Three types of vent systems are the masthead system, the standpipe system and the vapor recovery system (VRS). Schematic diagrams of all three types of recovery systems are presented in Figure 1. In a typical masthead system, groups of tanks are manifolded to a common header, with spill valves, pressure vacuum (PV) valves and flame arresters in the vent system line. In contrast, a standpipe system consists of a vertical pipe above each tank to release excess vapor to the atmosphere and allows inde-pendent venting of each tank. The pipe is usually goosenecked and equipped with a PV relief valve and flame control device. Vapor recovery systems are similar to the masthead system except additional piping is added to return the vented vapors to a shore disposal unit. These systems are employed to eliminate the emission of pollutant and toxic substances to the atmosphere.

All three types of vent systems present a finite resistance to the efflux of vapor when the PV valves are open. Vent pipes range in diameter from 2½" to 12" and are typically sized to accomodate the vapor displace-ment rates. The magnitude of resistance to gas outflow is many times less than that presented during liquid overfill when liquid cargo is flowing through the vent system. Further, it appears that vent systems

4

To Shoreside Recovery Unit
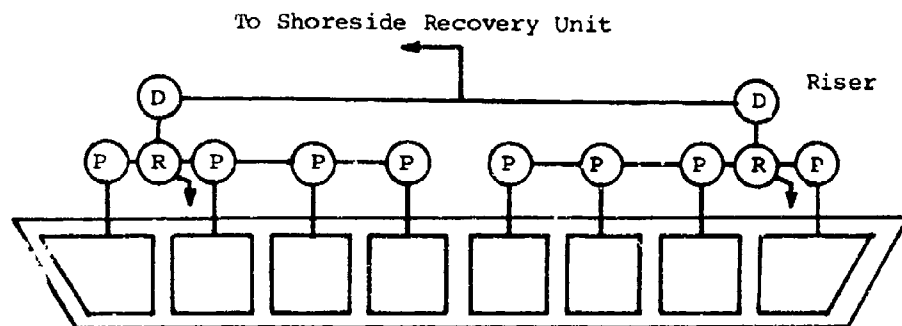
SCHEMATIC OF VAPOR RECOVERY SYSTEM
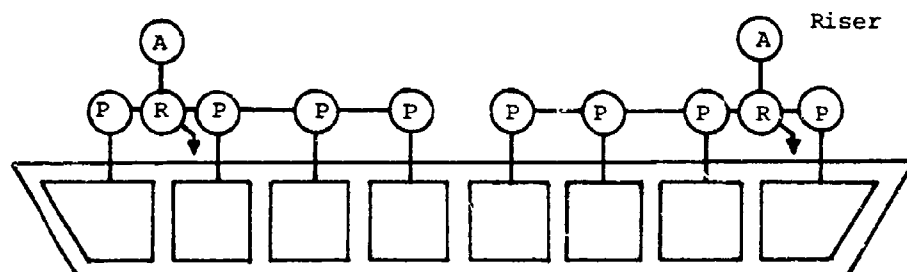
SCHEMATIC OF MASTHEAD SYSTEM
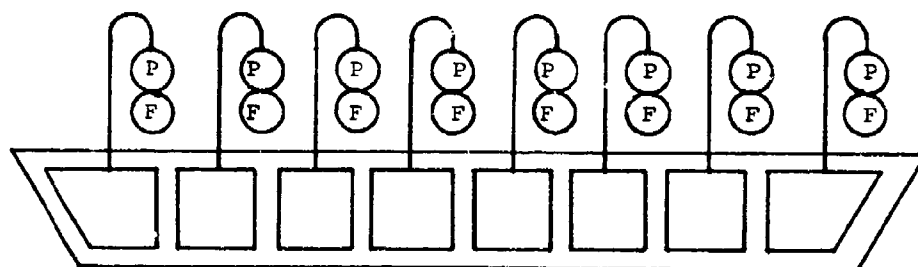
SCHEMATIC OF STANDPIPE SYSTEM

(D) DETONATION ARRESTOR

(P) PRESSURE VACUUM VALVE

(R) RELIEF OF SPILL VALVE

(F) FLAME SCREEN

(A) FLAME ARRESTOR

FIGURE 1 - SCHEMATICS OF TYPICAL VENT SYSTEMS (FROM REFERENCE 1)

5

designed for gas venting cannot handle the liquid overfill situation un-
less pumping rates are extremely low.

A convenient index of the resistance to either gas or liquid flow is
the effective length to diameter ratio (L/D) of the vent system. The L/D
of a vent system can .   at by summing the L/D ratios cf all the
pipe lengths employed i   .ystem and then adding in the appropriate
handbook L/D values for the various pipe fittings, valves, flame arrestors
or other items which comprise the overall L/D of the vent system. When
the L/D ratio is multiplied by the friction factor 4f (accounting for pipe
wall roughness and flow rate) the overall frictional resistance of the
vent system is established and can be employed in pressure drop calcula-
tions.

Due to the long lengths of pipe and the number of valves and arrestors
employed, vapor recovery systems have the highest L/D ratios. Length
to diameter ratios on the order of 1000 would not be unrealistic for a
typical VRS configuration, while a typical manifolded or standpipe vent
system would have an L/D ratio on the order of several hundred.

B. Factors Contributing To Pressure Rise

In general, typical vent systems can adequately discharge the vapor/
air mixture developed inside the tank without creating excessive tank
pressures (usually less than a few psig). However, in the case of an
accidental overfill, or a stuck valve, vent pipe blockage, or excessive
loading or evaporation rates, excessive tank pressures can occur. The
various factors important to pressure rise during normal cargo transfer
are depicted in Figure 2. As can be seen from Figure 2, the cargo being
loaded is evaporating as it is being loaded and the entering liquid

6
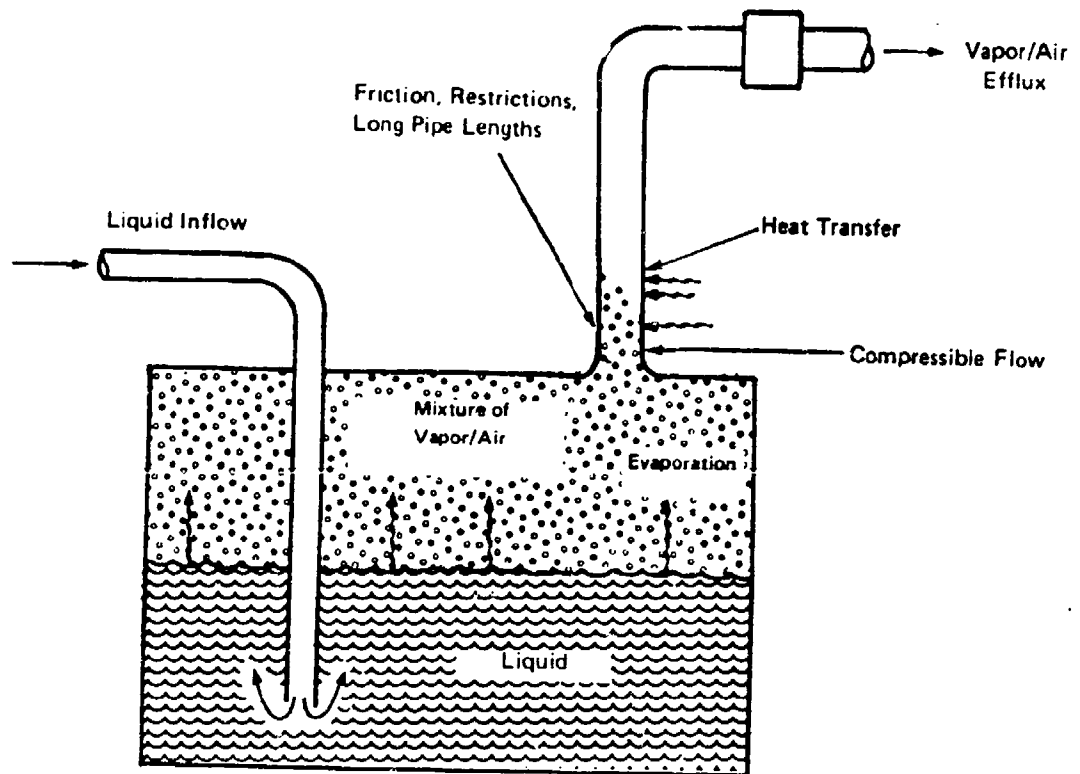
FIGURE 2   SCHEMATIC DIAGRAM SHOWING FACTORS IMPORTANT TO PRESSURE RISE
(FROM REFERENCE 1)

7

displaces the vapor/air mixture through the vent system. The finite resistance offered by the vent system to the efflux of the gas mixture creates the resulting pressure rise inside the tank. During liquid overfill it is the resistance of the vent system to liquid outflow that results in the pressure rise inside the tank.

As was stated earlier, overpressure can occur by inadvertent overfill, excessive loading rates, or inadequate vent system capacity. Some of the parameter values which constitute normal and extreme situations for cargo transfer are given in Table 1 (From Wilson and Raj, reference (1)). Further use of the terms normal or typical will re-lect the normal values.

Wilson and Raj[1] also made estimates of the minimum internal tank pressure loadings required to initiate failure of cargo tanks for three representative vessel designs: an offshore barge, an inland barge, and a large tankship. On the basis of the analyses of the three vessels, it has been calculated that an average internal pressure level in the cargo tanks of about 6 psig will be sufficient to initiate failure of the tank structure. This nominal pressure level represents the average of about 8 psig for the tankship, 6 psig for the offshore barge, and about 4 psig for the inland barge.

8

TABLE 1[*]

PARAMETER VALUES FOR NORMAL AND EXTREME TRANSFER OF CARGO

Parameter	Normal Range	Excessive Range	Notes
Tank fill time (tank volume/volumetric fill rate)	5 – 10 hr	1 – 5 hr	a
Inviscid vent pipe velocity (volumetric fill rate/vent pipe area)	20 – 40 ft/sec	40 – 200 ft/sec	b
Effective L/D	50 – 500	500 – 5,000	c
Friction factor 4f L/D	3 – 10	10 - 100	d
Cargo viscosity	1 – 100 cp	-	e
Cargo vapor pressure	0.1 – 10 psia	-	

Notes: (a) For example, 12,000 ft^3 barge tank filled at 1,200 - 2,400 ft^3/hr (150 - 300 gpm) or 60,000 ft^3 tank filled at 6,000 - 12,000 ft^3/hr (750 - 1,500 gpm). Excessive fill rates up to a factor of five above normal might be due to (a) wrong pump selection or (b) valves set for single tank loading rather than manifold of four tanks loaded at once.

(b) For example, 8,000 ft^3/hr displacement rate plus 1,000 ft^3/hr evaporation rate into 5 in. ID vent pipe gives 16 ft/sec efflux velocity (with P-V valve fully open).

(c) See Figure II-6. The standpipe vent of 6 in. ID has an L/D of about 170. The masthead vent has an L/D of about 470 for gas venting.

(d) Fanning friction coefficient f ≈ .005 according to Bird, Stewart, and Lightfoot, Transport Phenomenon, Wiley, p. 182ff.

(e) Viscosity is shown at an assumed 80°F loading temperature rather than at 100°F.

[*]From Reference 1

A. Analytical Models of Tank Pressure Rise

The rationale behind the development of the experimental models
can best be seen by first considering the analytical model of the physical
system and the factors important to pressure rise. Details of the deriva-
tion of the analytical model can be found in Wilson and Raj[1]. Briefly,
a mass balance equation was written for the vapor mass in the tank as a
function of the outflow rate and the cargo evaporation rate:

$$\frac{dM}{dt} \;=\; -\dot{M}_v \;+\; \dot{M}_{vap} \tag{1}$$

| Rate of change of air/vapor mass in the tank | Mass rate of venting | Mass added from evaporation |

Equation (1) is the basic equation describing the pressure rise in-
side the tank. Then, by deriving an expression for the evaporation rate
and taking into account the pumping rate, vent system hydraulics and the
fluid characteristics, the following equation was arrived at describing
the rate of pressure rise in the tank:

$$t_{fill}(1-t/t_{fill})\ \frac{d(p/p_a)}{dt} = p/p_a + K\left(\frac{t_{fill}}{t}\right)^{\frac{1}{2}} - \frac{\left[(p/p_a)^2 - 1\right]^{\frac{1}{2}}\ \sqrt{RT}}{(\dot{Q}/A)\ [2\ln(p/p_a)+4f\ L/D]^{\frac{1}{2}}} \tag{2}$$

where:

t_{fill} = tank fill time (tank volume/loading rate)

t = time

p = tank top pressure

p_a = atmospheric pressure

K = ratio of evaporation rate to loading rate, taken at t_{fill}

10

R = gas constant

T = temperature

$\dot{Q}$ = loading rate

A = vent pipe cross sectional area

f = fanning friction factor

L/D = length to diameter ratio of the vent system

Equation (2) is subject to the initial condition $p/p_a = 1$ at $t = 0$ and can be numerically integrated. The key independent parameters in equation (2) are $\dot{Q}/A$, K, $4f\ L/D$ and t/t_{fill}.

Formulation of the analytical model for the case of liquid overfill was approached in the same manner as that for the normal transfer case. The physical factors for modeling the tank pressure rise during liquid overfill are shown in Figure 3. When the tank becomes liquid full, continued pumping begins to displace liquid into the vent system. The frictional pressure drop from the vent system in addition to the liquid head it imposes, creates the pressure buildup in the cargo tank. The tank/vent system attempts to relieve the pressure drop by compression of the liquid and expansion of the tank walls.

To analytically model liquid overfill, a mass balance for the tank-liquid system is first written:

$$\underbrace{\frac{dM}{dt}}_{\substack{\text{Rate of accumulation} \\ \text{of mass} \\ \text{within the tank}}} = \underbrace{\dot{M}_i}_{\substack{\text{Inlet mass} \\ \text{flow rate} \\ \text{of liquid}}} - \underbrace{\rho A U}_{\substack{\text{Outflow rate} \\ \text{of liquid} \\ \text{from the tank}}} \qquad (3)$$

where ρ is fluid density, A is the vent cross section area, and U

11

t = 0
Cargo Fills Tank

Friction

Tank Walls Expand

Vertical Head

Liquid
Compresses

Additional Pressure Drop
From Fittings

t = 1 - 10 sec.
Cargo Enters Vent

t = 20 - 200 sec.
Cargo Fills
Vent System
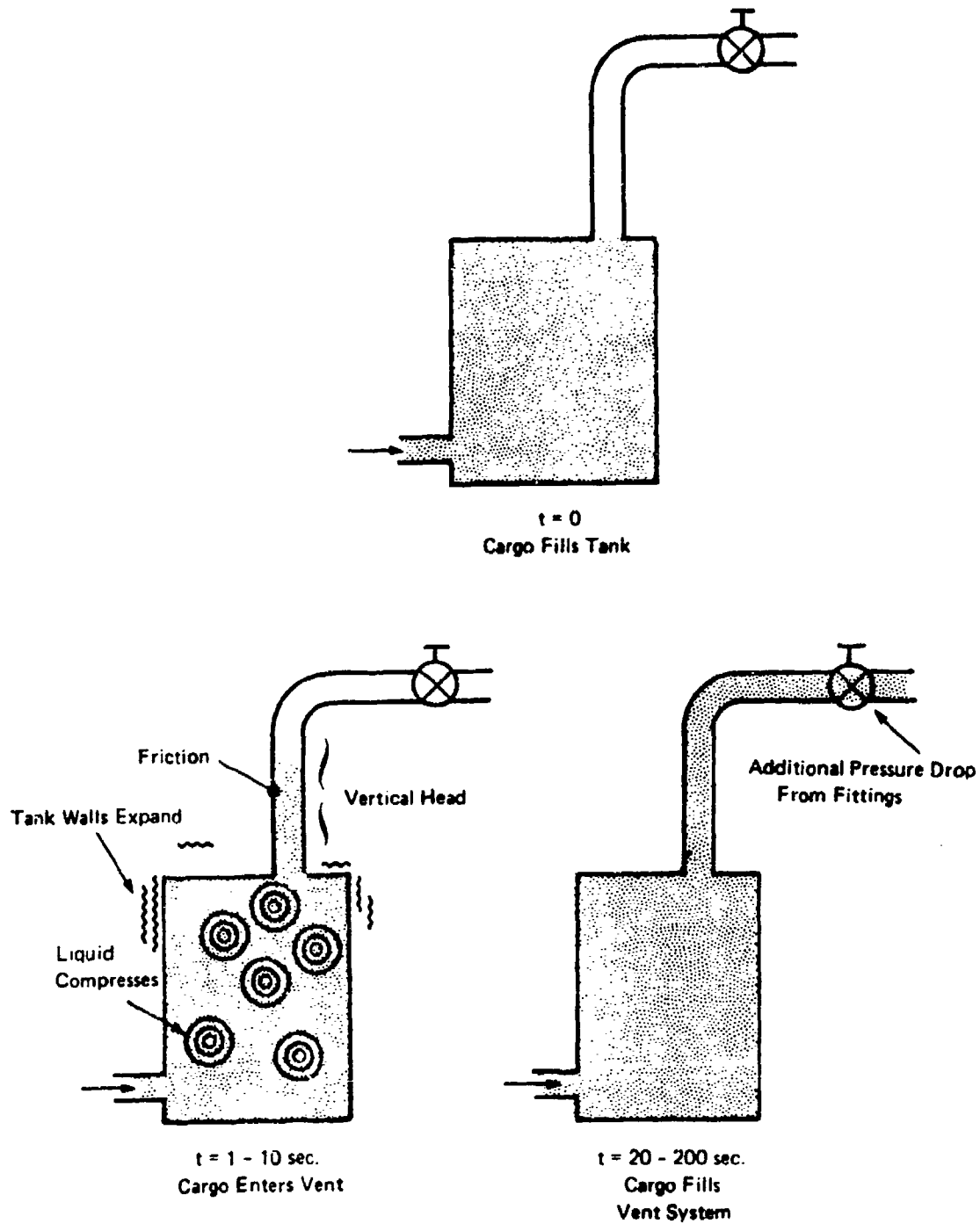
FIGURE   3   SCHEMATIC OF THE PHYSICAL SYSTEM FOR
MODELING THE TANK PRESSURE RISE
DURING OVERFILL (Wilson and Raj(1))

is the mean velocity of liquid in the vent pipe. Now, the hydraulics of the vent system, the compressibility of the liquid, the cargo loading rate, and the tank geometric and structural characteristics are employed to arrive at the following governing equation for liquid overfill:

$$\frac{dp}{dt} = \frac{1}{(B + \chi)} \left[\frac{(\dot{Q}/A) - U}{(V_T/A) + (\dot{Q}/A)\, t - \int_o^t U\, dt} \right] \tag{4}$$

where:

B = coefficient of volume expansion of the tank by pressure $(= \frac{1}{V_T}\frac{dV}{dp})$

χ = compressibility of liquid = $\frac{1}{\rho}\frac{d\rho}{dp}$

V_T = tank volume

and all other terms are as previously defined. This basic equation for overfill employed the following assumptions for analytical solutions.

(1) Constant mass inflow rate $\dot{M}_i$

(2) Constant values of B and χ

(3) Fully turbulent pipe flow

Equation (4) is rather cumbersome and an iterative procedure must be employed to obtain p and U as functions of time. The case of a blocked vent provides a conservative estimate of the time required to reach maximum allowable pressure for normal and high loading rates during overfill. Assuming U = O (vent blocked) equation (4) becomes:

$$p - p_a = \frac{1}{(B + \chi)} \ln \left(1 + \frac{\dot{Q}}{V_T}\, t \right) \tag{5}$$

Safe rates at which overfill can be sustained can be found by assuming a steady flow condition $(\dot{Q}/A = U)$ for the vent system. Then the tank pressure can be related to the mass outflow rate and solved for the liquid efflux velocity U:

13

$$\dot{Q}/A = U = \left[\frac{p-p_a-\rho g H}{4\, \rho\, [4f\, L/D+1]} \right]^{\frac{1}{2}}$$

(6)

where H is the maximum height of the vent system above the tank top. By substituting the maximum allowable gage pressure ($p-p_a$) that a tank can withstand into equation (6), one would be able to arrive at the maximum allowable ratio of loading rate to vent cross sectional area ($\dot{Q}/A$) that a tank is capable of receiving for an overfill situation without failing.

B. Experimental Model for Normal Transfer

Physically, the test fixture consisted of pumps and flowmeters for air and water, a model tank and vent system, and various pressure, strain and deflection transducers arranged in the manner shown in Figure 4. The model tank is a 55 gallon drum and the model vent system is 3/16 inch inner diameter high pressure tubing mounted in one of the drum bungs. It should be noted that the analytical model for normal transfer is in no way dependent on tank geometric or structural characteristics. The choice of a 55 gallon drum for the model tank was based on economy, convenience, and on the drum coefficient of volume expansion B, which governs the rate of pressure rise for liquid overfill. The value of B for the model tank is .000388 psi^{-1} which is within the range of B values for typical tanks (.001 to .00001 psi^{-1})[1].

Examination of equation (2) shows the pressure rise inside the tank to be a function of the quantities $\dot{Q}/A$, $4fL/D$, t/t_{fill}, RT and K (for the case of K≠0). Thus for any experimental model study, if these quantities are held the same in the model as in the prototype, the resulting pressures

14

VENT PIPE - SIMULATES 4fL/D
OF ENTIRE VENT SYSTEM

PRESSURE TRANSDUCER

AIR FLOWMETER

$\dot{M}_{VAP}$ AIR PUMP

STRAIN GAGES
ON MODEL TANK

$\dot{Q}$ WATER PUMP

WATER
FLOWMETER

LINEAR POTENTIOMETERS
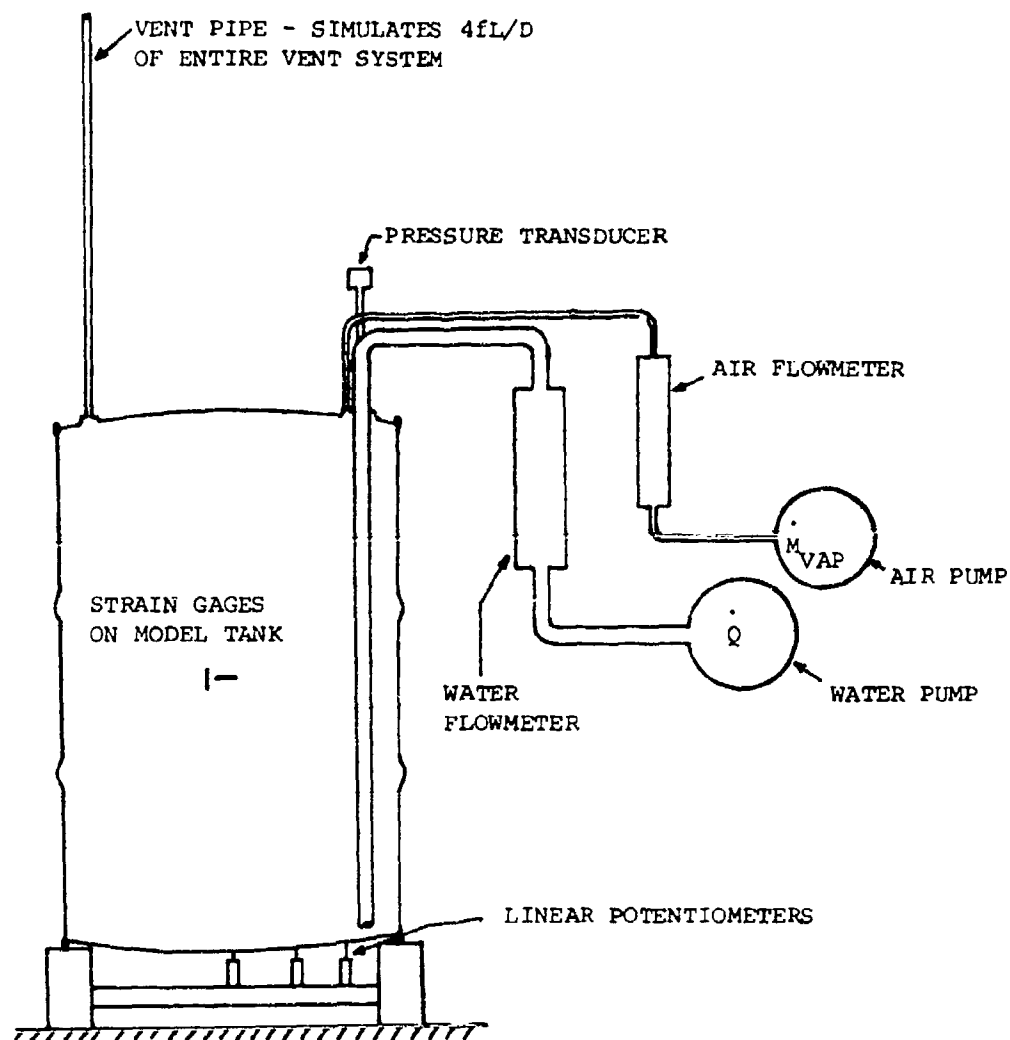
FIGURE 4 - SCHEMATIC OF EXPERIMENTAL MODEL

15

in the model and prototype will be identical for the same values of t/t_{fill}.
The modeling of each of the above parameters was accomplished as follows:

(1) Gas Properties (RT) - The analytical model assumes that the vapor-air mixture being vented has the same molecular weight, specific heat and viscosity as that of pure air. Thus, an experimental model venting air at the same rate at which the vapor-air mixture is vented in the analytical model would suffice for the validation of the analytical model.

(2) Vent Pipe Efflux Velocity ($\dot{Q}/A$) - This term is expressed as the ratio of the tank loading rate to vent cross sectional area, and serves as a convenient way to express a nominal efflux velocity based on operational and design guidelines. Thus, by manipulating this ratio ($\dot{Q}/A$), the effects of different loading rates on tank pressure can be examined, with the resulting experimental model tank pressures being the same as those that would be expected for a real life situation with the same $\dot{Q}/A$ ratio.

(3) Vent System Frictional Flow Resistance - This parameter is taken into account in the term 4f L/D. Thus, for a given vent cross section area (defines D) and knowing the relative roughness of the model vent pipe (establishes 4f), one can then employ different lengths of pipe in the tank/vent system model to evaluate the quantity 4f L/D. Establishing the model vent pipe relative roughness and relating it to the fanning friction factor (4f) was accomplished in a seperate determination and is detailed in Appendix A. Obviously, the flow in the vent system must be in the same regime (e.g., turbulent) for both the experimental and analytical models. Also, subsonic flow must be maintained.

16

(4) Cargo Evaporation Rate - Cargo evaporation during the loading of volatile cargo was simulated by pumping air into the model tank at a mass rate described by the analytical model for cargo evaporation (equation (5), Reference 1). The mathematical expression governing evaporation in the analytical model is given as:

$$\dot{M}_{vap} = K \rho_a \dot{Q} (t_{fill}/t)^{\frac{1}{2}}$$

(7)

and is illustrated in Figure 5 for a loading rate $Q/A = 100$ ft/sec and evaporation rate to loading rate ratio of $K = .2$. The term K, the ratio of the cargo volumetric evaporation rate ($\dot{M}_{VAP}/\rho_{VAP}$) to loading rate $\dot{Q}$ is simply a means of relating the evaporation rate to the loading rate at a particular time ($t = t_{fill}$) since the evaporation rate changes with time.

The following assumptions apply to the analytical evaporation model and would likewise apply to any experimental results where evaporation is considered:

(1) The density of pure vapor is the same as that for pure air $(\rho_a = \rho_{VAP})$.

(2) Cargo loading temperature is close to ambient

(3) The liquid surface stays at the cargo loading temperature and has a constant area equal to the area of the tank floor.

Also shown in Figure 5 is the experimental simulation of the analytical evaporation model for the same cases. The problem of $\dot{M}_{VAP}$ going to infinity when $t=0$ was approximated by setting the air flow rate to the maximum amount the air flowmeter could accurately monitor until an $\dot{M}_{VAP}$ value was reached which corresponded to an amount predicted by the analytical model. The analytical curve was then approximated in the stepwise

17
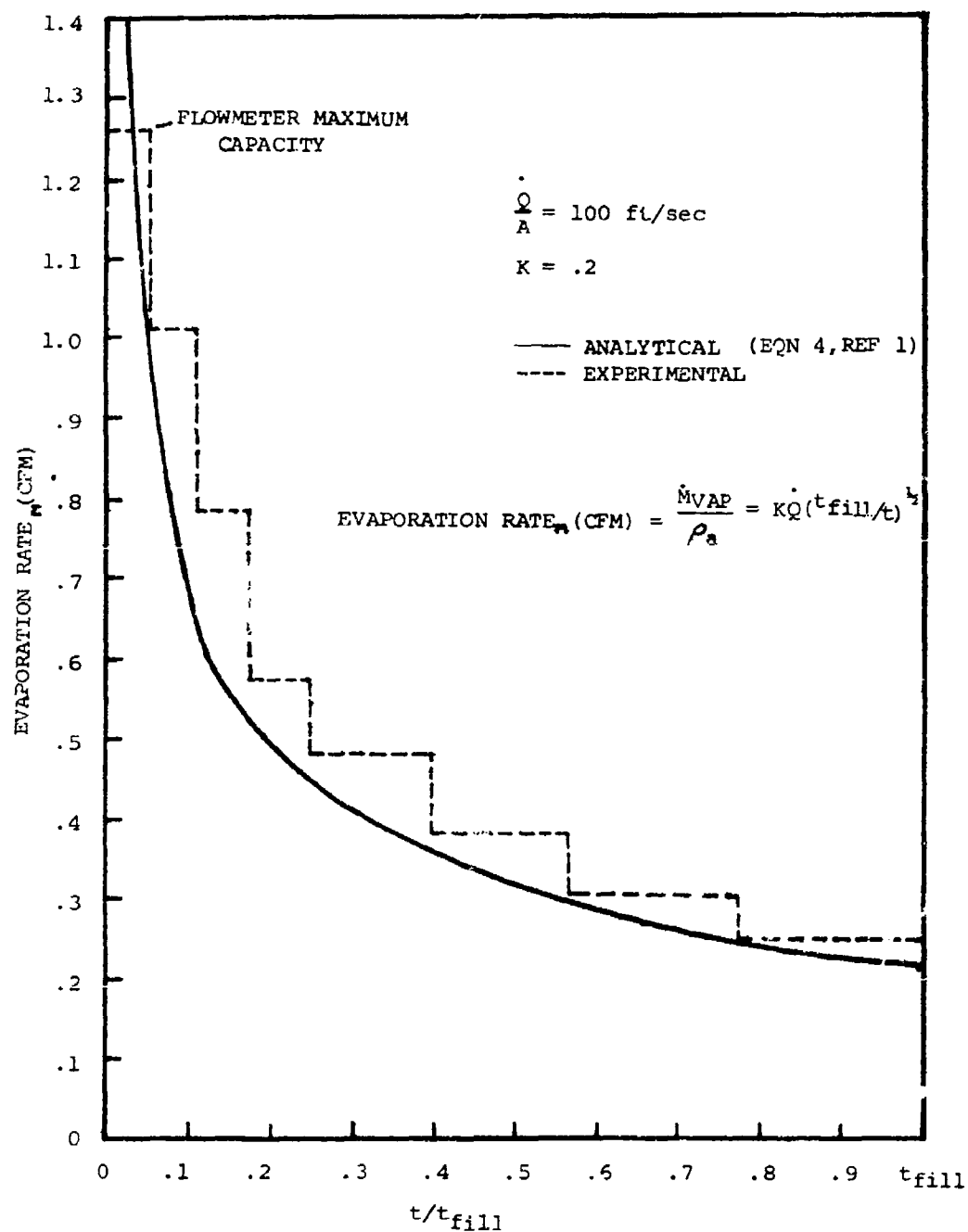
FIGURE 5 - ANALYTICAL AND EXPERIMENTAL MODELS OF CARGO EVAPORATION

18

manner shown in Figure 5. Additionally, the pumping of air to simulate evaporation is consistent with the assumption in the analytical model that pure air is being vented through the vent system.

Then, with the above quantities modeled as described, one would obtain tank pressures in the model which would be the same as prototype pressures that would be realized in a prototype with the same values of the independent parameters $4fL/D$, $\dot{Q}/A$, and K, at equal values of t/t_{fill}.

C. Experimental Models for Liquid Overfill and Blocked Vent

The model for liquid overfill is physically the same as that for the case of normal transfer. One will note from equation (4) that the rate of pressure rise for liquid overfill is a function of loading rate $\dot{Q}$, tank volume V_T, liquid compressibility $\mathfrak{H}$, vent area A, the tank's coefficient of volume expansion B and the velocity of liquid in the vent system U, which is itself a function of p and the physical configuration of the vent system (i.e. $4fL/D$ and H, the vent system resistance and height respectively). It can be shown that for mos t ks, the bulk modulus B is much larger (less stiff) than the compressibility of the liquid (B>>$\mathfrak{H}$), therefore B is the more influential of these two terms in governing the rate of pressure rise. Then, if one were to select a model tank with a value of B similar to that for a typical cargo tank, in addition to ratios of loading rate to tank volume ($\dot{Q}/V_T$), loading rate to vent area ($\dot{Q}/A$), $4fL/D$ and H which correspond to typical cargo operations, one would obtain a model pressure-time history which would correspond exactly to a typical cargo tank pressure-time history with the same values of $\dot{Q}/V_T$, $\dot{Q}/A$, $4fL/D$, H and B. The terms $4fL/D$ and H, while not in equation (4), along with p determine the rate of liquid flow in the

19

vent U. Thus, any comparison between experimental and analytical results for liquid overfill, should take into account the vent system parameters 4fL/D and H to have a meaningful comparison. Additionally, it is worth noting that the pressure-time relationship in model and real life for liquid overfill is based on the time after the tank becomes liquid full, and not the non-dimensionalized fraction of total fill time as in the case of normal transfer.

Thus, a model tank was needed which possessed structural characteristics resulting in a modulus of pressure/volume expansion within the range of typical moduli one would find for an actual cargo tank. After investigating various possibilities, it was determined that a 55 gallon drum possessed these characteristics. Since 95% of the volume change of the drum from pressure occurs in the drum's top and bottom, it was imperative that the drum top and bottom plate deflections be measured accurately. To accomplish this, the Moiré Contour Sum-Contour Difference Method (References 2 and 3) was used to measure the plate deflections, and was backed up by linear potentiometers mounted on the drum top and bottom. The Moiré technique determines changes in surface elevation and hence volume, by observing contour-like patterns created by the mode interference of a grid with its shadow cast onto a surface and comparing the interference patterns for different deformed states. The Moiré method was employed both statically (to calibrate) and dynamically (during overfill tests), for determining the volume changes in the tank with pressure. Details on the technique and results from the Moiré evaluations can be found in Appendix B.

20

Simulation of a blocked vent was accomplished by installing a ball valve in the vent pipe opening and closing it after overfill had begun. As can be observed from the analytical formulation for a blocked vent, equation (5), the rate of pressure rise is a function of the tank bulk modulus (B), liquid compressibility (λ) and the ratio of loading rate to tank volume ($\dot{Q}/V_T$). By modeling these parameters in the same manner as was done for liquid overfill, pressure-time histories the same as those expected from a prototype with the same parameters would be obtained. Additionally, since the model tank was rated for a maximum internal pressure of 40 psig, all liquid overfill evaluations were terminated at an internal model tank pressure of 25 psig.

IV. PRESSURE HISTORIES LOADING CARGO

A. Loading Non-Volatile Cargo

The effect of loading a non-volatile cargo was simulated by pumping water into the test tank at a rate to produce the desired $\dot{Q}/A$ ratio and monitoring the tank pressure buildup. The effects of vent restriction (4f L/D = 10, 20, 35) and loading rate ($\dot{Q}/A$ = 30, 50, 100, 150 ft/sec) with no cargo evaporation (K = 0) were examined. Figures 6 and 7 show the pressure rise under the conditions of $\dot{Q}/A$ = 100 ft/sec and 4f L/D = 10 and 4f L/D = 20 respectively. The tank top pressure (psig) is plotted against the fraction of total fill time in these figures. Also included in Figure 6 is the pressure-time history as predicted by the analytical model. One can observe from both figures the good repeatability the experimental results exhibited from run to run and also note the good correlation with the analytical results. There is a slight discrepancy between experimental and analytical values in the early stages of loading, but the important point to note in Figure 6 is that both analytical and experimental models predict the same maximum pressure that will be realized for the loading operation.

Equation (2), which describes the rate of pressure rise as a function of time must be numerically integrated and is therefore not well suited for practical use. A similar, but less complicated solution to equation (2) when considering non-volatile cargoes can be arrived at by letting $t = t_{fill}$ and K = 0 to arrive at an expression which describes the tank top pressure for loading cargo with no cargo evaporation as was done to arrive at equation (8).

22
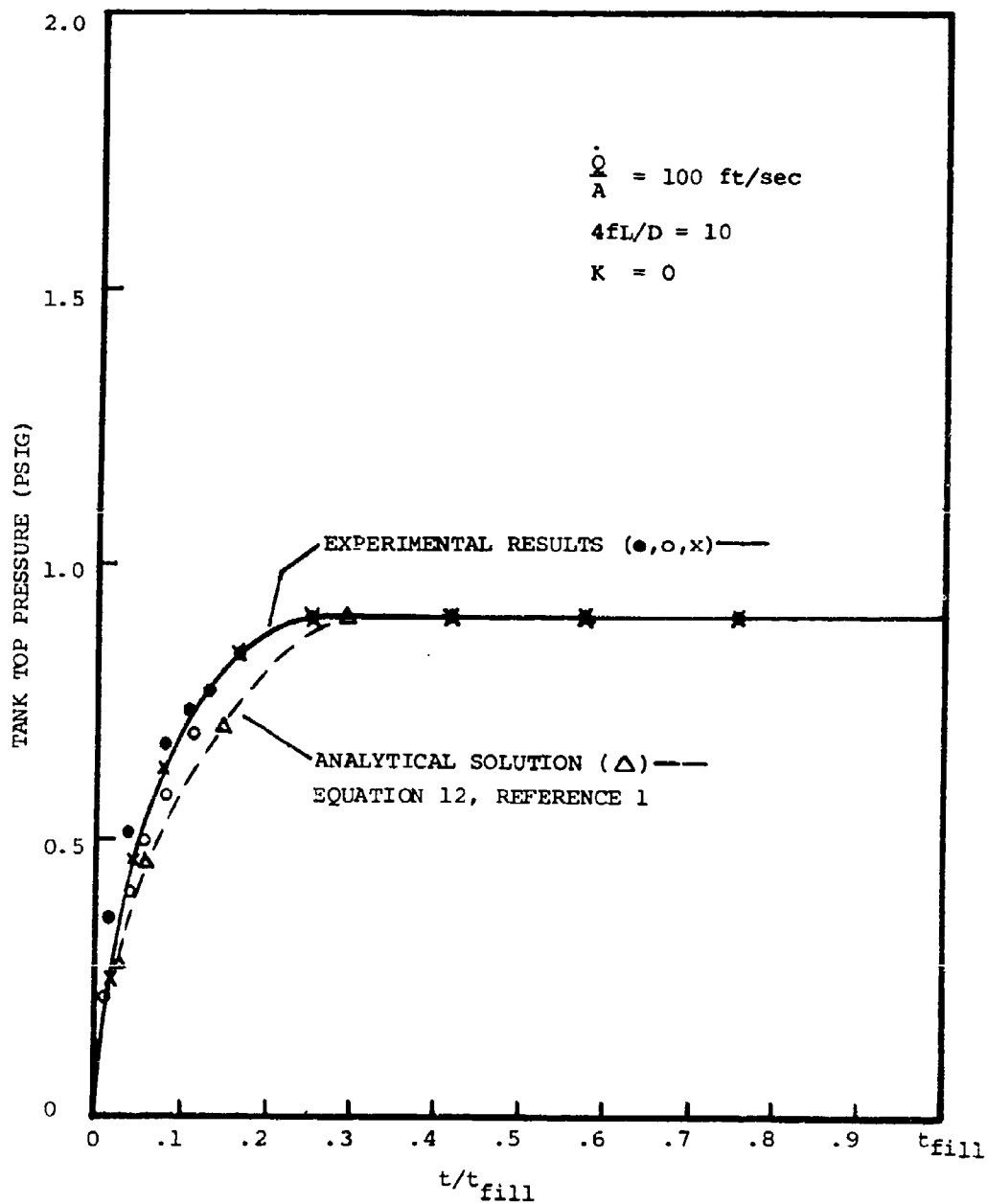
FIGURE 6 - PRESSURE vs FRACTION OF TOTAL FILL TIME LOADING CARGO

23
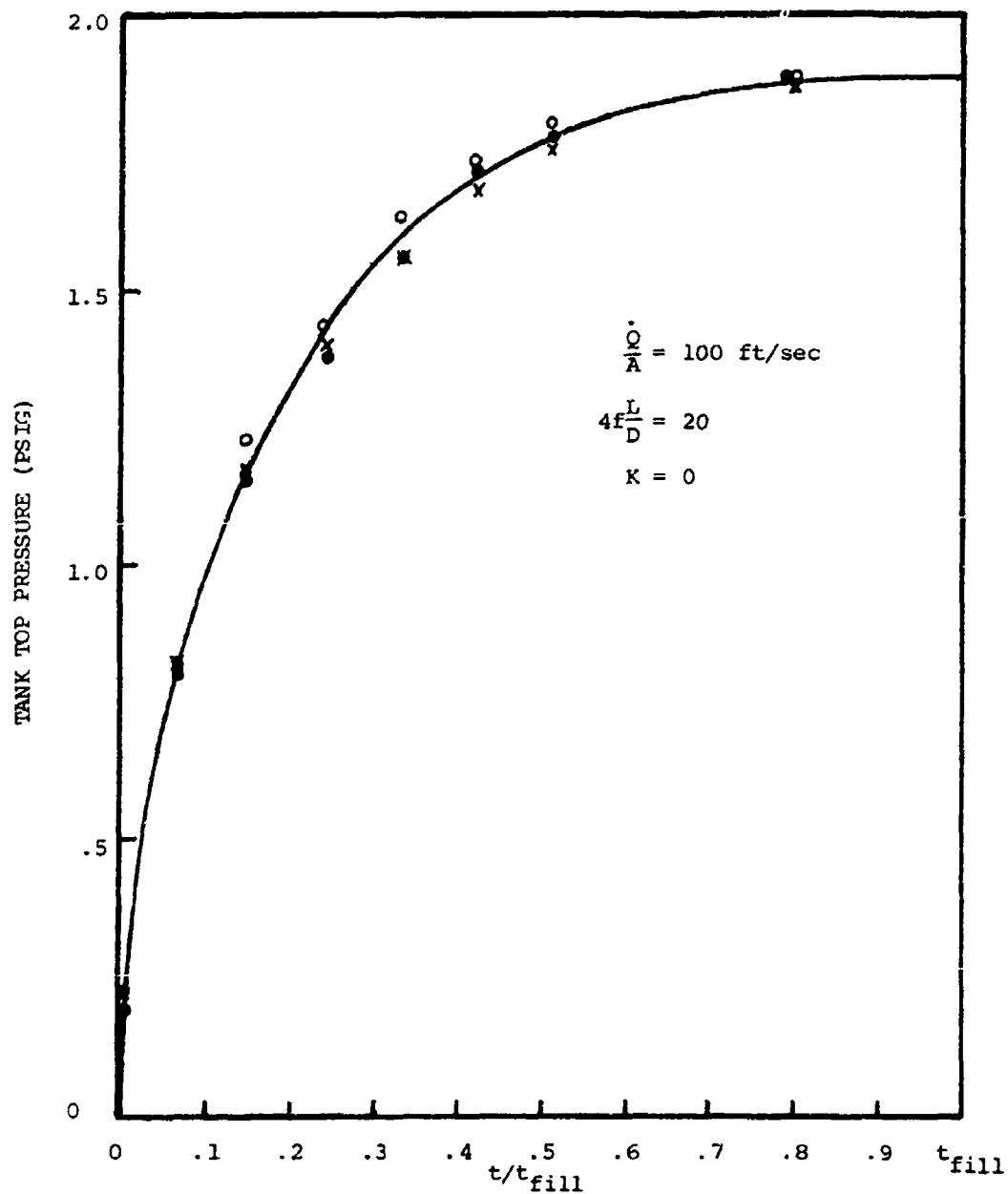
FIGURE 7 – PRESSURE vs FRACTION OF TOTAL FILL TIME LOADING CARGO
FOR EXPERIMENTAL MODEL

24

$$\frac{p}{p_a} = \left[\frac{RT}{RT - (Q/A)^2\left[2\ln(p/p_a)+4fL/D\right]}\right]^{\frac{1}{2}} \qquad (8)$$

Equation (8) predicts the tank top pressure at $t = t_{fill}$, which experimental and analytical pressure-time histories indicate is the maximum pressure that will be attained for a loading operation with no cargo evaporation. Equation (8) cannot be solved directly, but must be iterated to arrive at a solution. The iterative process is hastened by first solving equation (8) for p/p_a without the term $2\ln(p/p_a)$ in the denominator and then using the value of p/p_a in the complete expression to generate a new p/p_a . Convergence is rapid since $2\ln(p/p_a)$ is small compared to $4f$ L/D. Table 2 gives the experimentally arrived at maximum pressures for the loading rates and vent restrictions examined. Also included in Table 2 are the maximum predicted pressures using equation (8). The correlation between analytical and experimental results is considered good and certainly within the bounds of experimental error.

Figure 8 illustrates the relationship between the maximum absolute gage pressure that would be realized for a particular transfer rate ($\dot{Q}/A$) and vent system ($4f$ L/D) as predicted by equation (8). From Figure 8 it is evident that with higher loading rates and vent system frictional resistances, one need only vary the loading rate slightly to produce large changes in the maximum pressure attained, implying pumping rates must be accurately monitored or that these rates must be avoided to diminish the risk of accidental overpressurization. Further, $4f$ L/D is subject to change (increase) as corrosion develops in the vent system. Therefore,

25

TABLE 2

ANALYTICAL AND EXPERIMENTAL MAXIMUM PRESSURES
LOADING NON-VOLATILE CARGO

$$P_{max} \text{ (psig)}$$

$\dfrac{\dot{Q}}{A}$ (ft/sec)		NOMINAL $4f\dfrac{L}{D}$		
		*(ACTUAL) 10	*(ACTUAL) 20	*(ACTUAL) 35
30	Experimental / Analytical	.10 (12.6) / .09	.14 (25.2) / .19	.17 (44.2) / .34
50	Experimental / Analytical	.25 (11.4) / .24	.52 (22.8) / .49	.75 (41.0) / .92
100	Experimental / Analytical	.90 (10.0) / .90	1.90 (19.5) / 1.97	3.80 (34.0) / 4.02
150	Experimental / Analytical	1.95 (9.2) / 2.12	4.57 (18.1) / 5.44	**

* Actual $4f\dfrac{L}{D}$ value used experimentally and for calculations (see Appendix A).

** Loading rate and vent restriction combination produce choked flow.

26
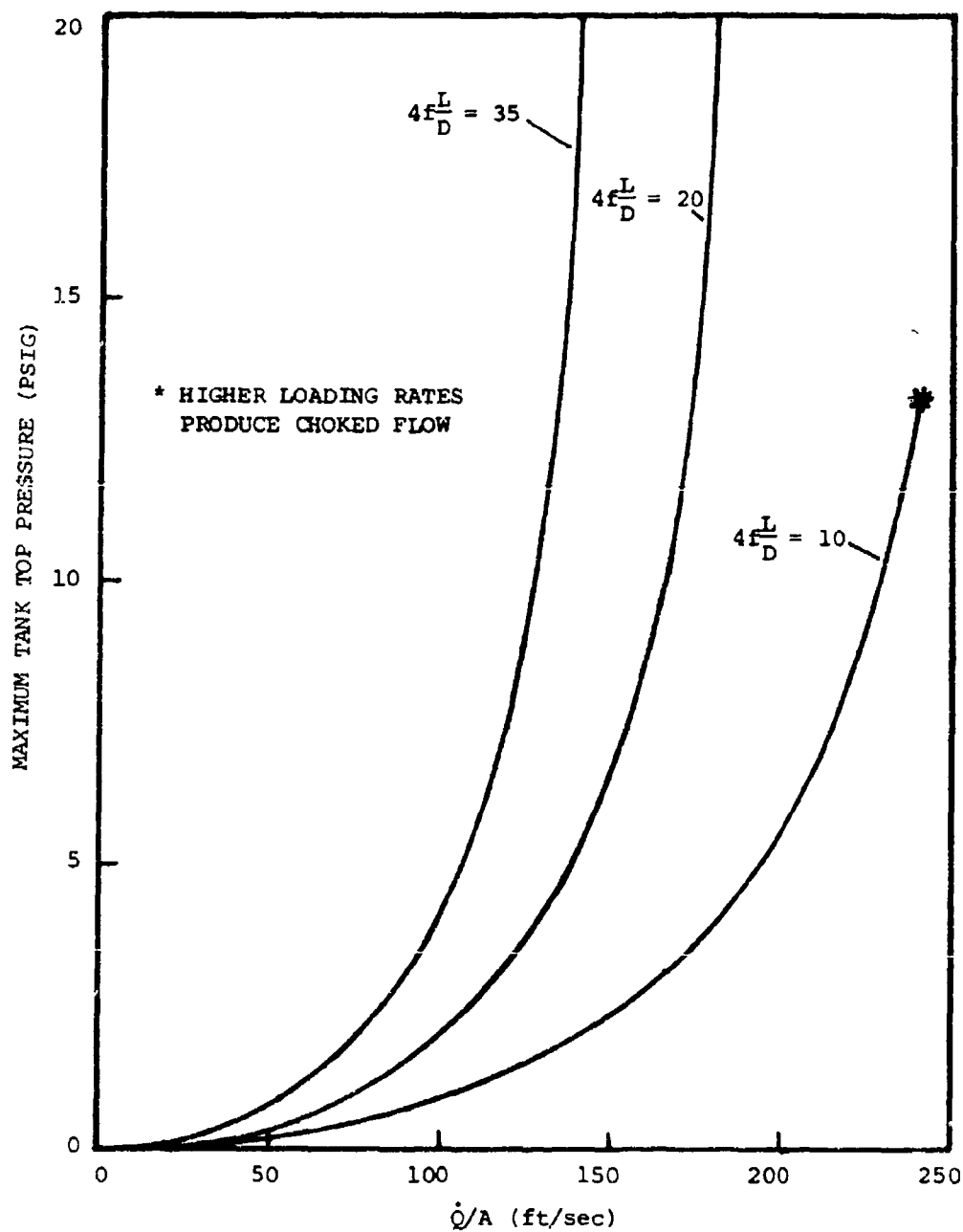
FIGURE 8 - MAXIMUM TANK TOP PRESSURE vs TRANSFER RATE
LOADING NON-VOLATILE CARGO FOR ANALYTICAL
MODEL (EQUATION 8)

27

safe loading rates for a given system may become unsafe in time as corrosion may increase the value of 4f L/D.

From the analyses and results, the following conclusions were reached for loading non-volatile cargoes:

(1) Maximum tank top pressures resulting from loading cargo without evaporation are sufficiently low so as to provide an adequate safety factor for currently employed loading rates and tank structures ($\frac{\dot{Q}}{A}$ = 80ft/sec, 4f $\frac{L}{D}$ = 20).

(2) Maximum tank top pressures occur at t = t_{fill} for loading cargo with no cargo evaporation, and can be calculated using the simplified expression, equation (8).

B. Loading Volatile Cargo

Loading cargo with the cargo evaporating into the tank was simulated by simultaneously pumping air and water into the model tank as described previously. The following parameter values were examined to assess the effects of cargo evaporation:

Vent restriction = 4f L/D = 10, 20

$\frac{\text{Loading Rate}}{\text{Vent Area}}$ = $\dot{Q}$/A = 30, 50, 100 ft/sec

$\frac{\text{Evaporation Rate}}{\text{Loading Rate}}$ = K = 0.2, 0.5

In general, the effect of cargo evaporation is to increase the maximum tank pressure realized for a given vent restriction and loading rate. Comparing the experimental results presented in Figures 9 and 10 shows the effects of increasing evaporation and loading rates on the pressure-time history. Equation (2) shows that dp/dt is greater for evaporation than non-evaporation cases. Figure 11 compares pressure-time histories generated

28
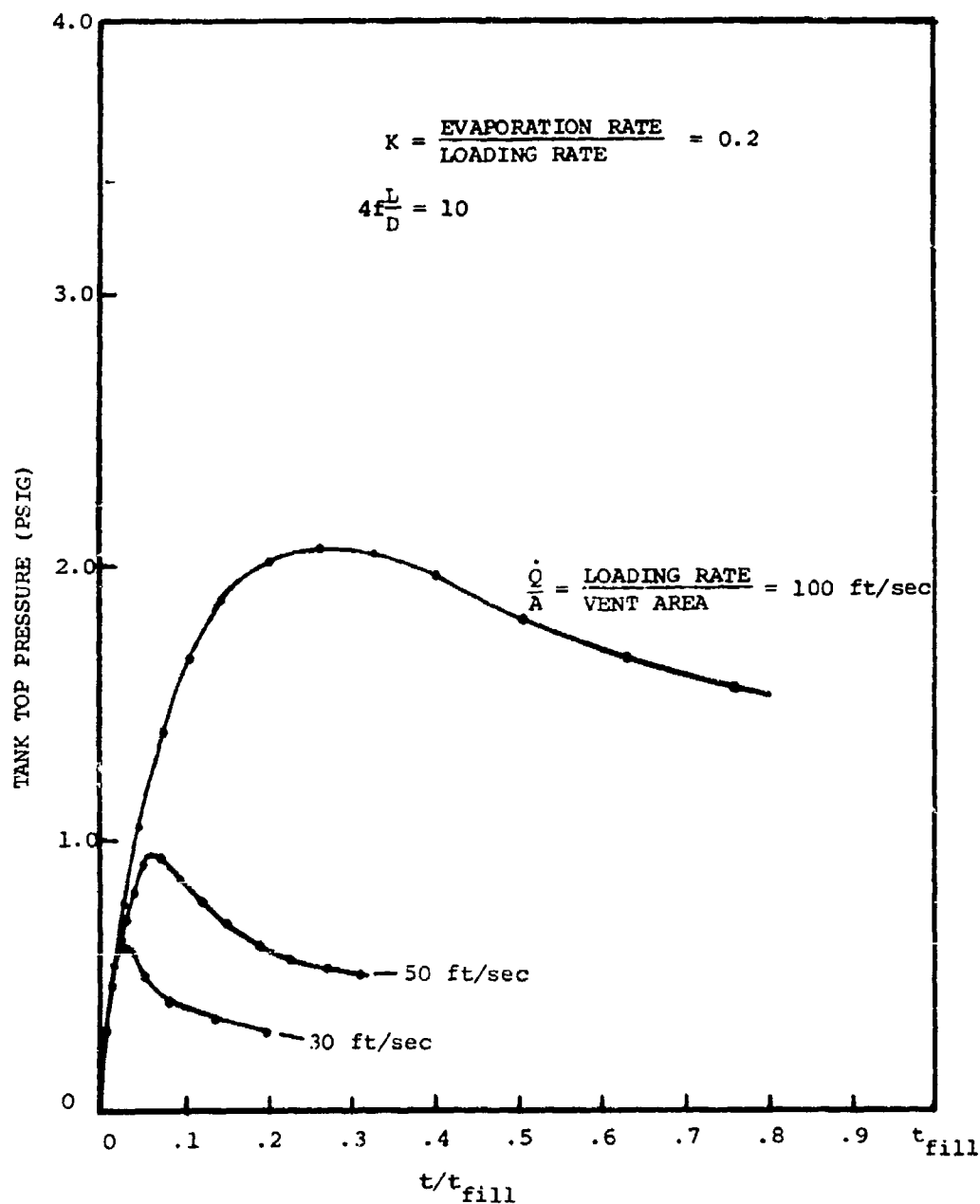
FIGURE 9 – EFFECT OF LOADING RATE ON PRESSURE – TIME
HISTORY LOADING VOLATILE CARGO FOR
EXPERIMENTAL MODEL
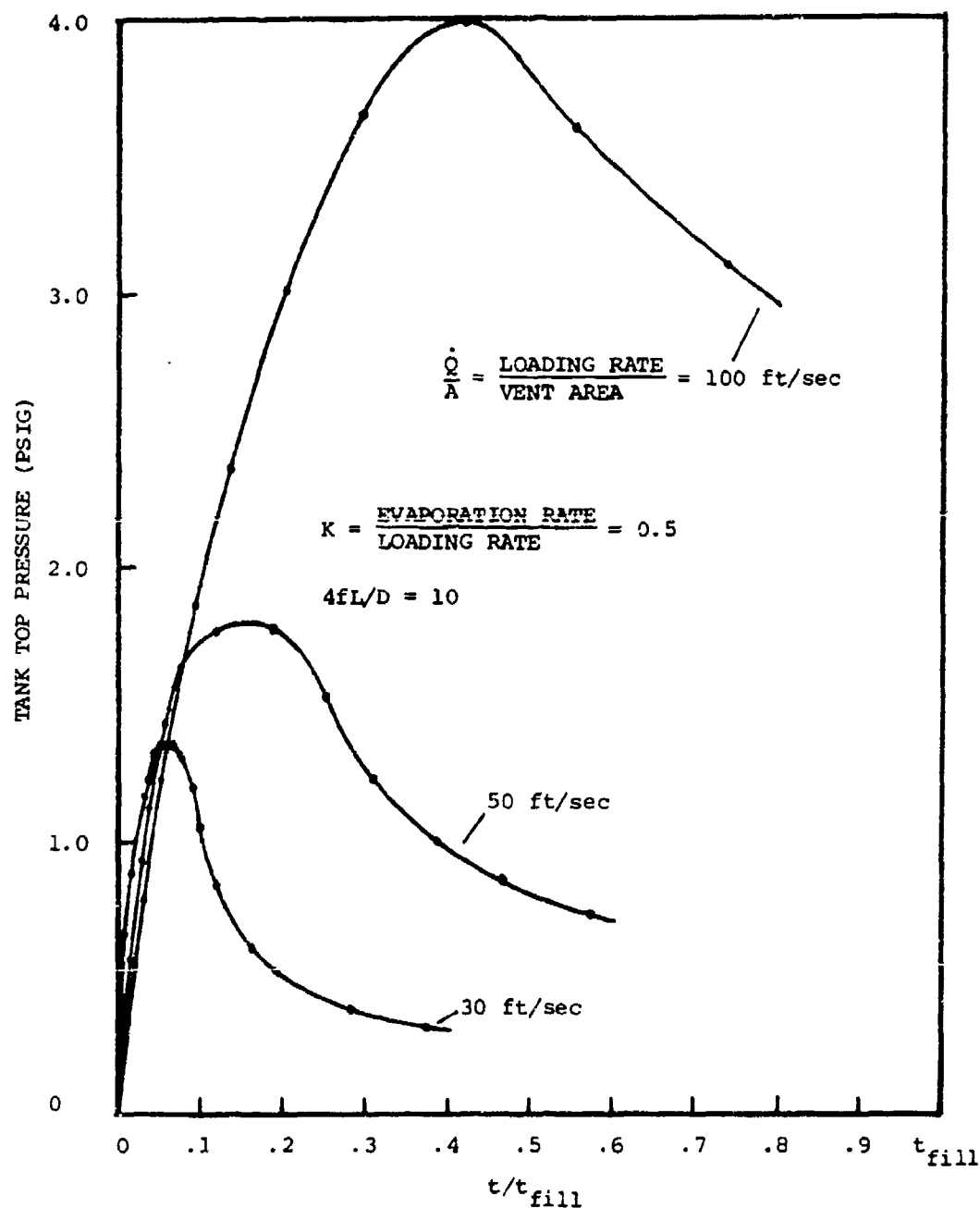
FIGURE 10 - EFFECT OF LOADING RATE ON PRESSURE - TIME
HISTORY LOADING VOLATILE CARGO FOR
EXPERIMENTAL MODEL

30

by the analytical and experimental models when considering cargo evaporation. The results shown in Figure 11 are for typical evaporation and loading rates and are indicative of the repeatability of the experimental results and the correlation attained with analytical data.

The results of the experimental evaluations of loading cargo with cargo evaporation are summarized in Table 3. Table 3 gives the maximum tank top pressures attained loading cargo at various transfer rates, evaporation rates and vent system restrictions. One will note that the maximum tank top pressures attained are below the tank failure pressures calculated for typical cargo tanks with the exception of the case where $\dot{Q}/A = 100$ ft/sec, $K = .5$ and $4f$ $L/D = 20$, which combines high evaporation and loading rates. Thus, one can conclude that the danger of tank overpressure during normal cargo transfer with typical vent restrictions and transfer and evaporation rates is small and will only occur if one or more of these parameters becomes excessive.

C. Summary of Results Loading Cargo

The experimental results obtained for loading cargo are summarized in Figures 12 and 13 as plots of maximum tank top pressure vs. cargo trasfer rate for specific vent restrictions and evaporation rates. Also included in Figure 12 are the analytical results for the parameter values corresponding to the experimental results, again demonstrating the good correlation between the two. The regime of expected tank failure is also indicated in each figure and one will observe that it takes a combination of high loading and evaporation rates to approach a tank pressure that is considered unsafe.

31
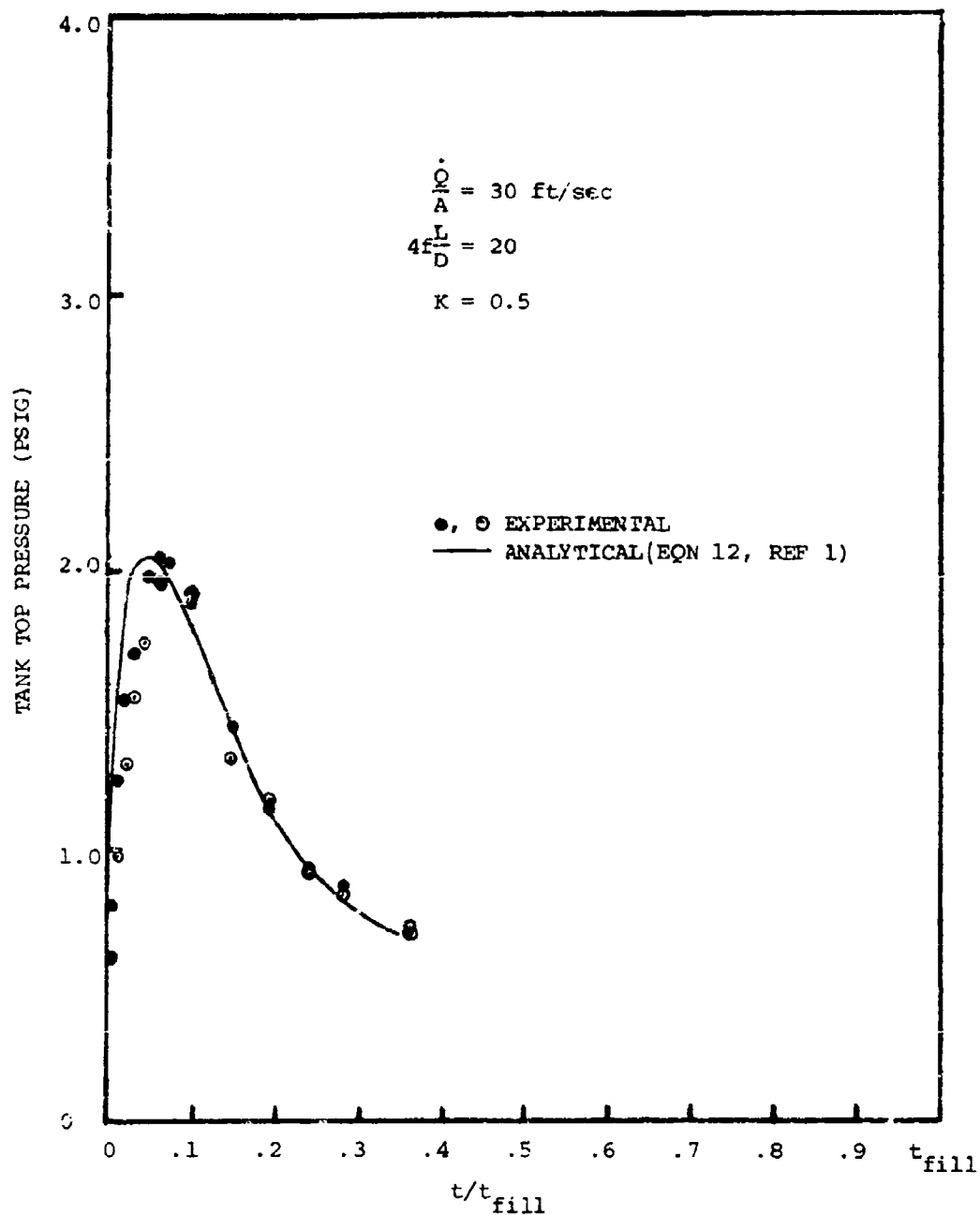
FIGURE 11 - COMPARISON OF EXPERIMENTAL AND ANALYTICAL
RESULTS LOADING VOLATILE CARGO

32

TABLE 3

EXPERIMENTAL MAXIMUM PRESSURES LOADING
VOLATILE CARGO

P_{max} (psig)

Q/A = 30 ft/sec

K	NOMINAL $4f\frac{L}{D}$		*(ACTUAL)
	10	20	
0.2	.58 (11.9)	.74 (23.9)	
0.5	1.31 (11.4)	2.06 (22.8)	

Q/A = 50 ft/sec

K	NOMINAL $4f\frac{L}{D}$		*(ACTUAL)
	10	20	
0.2	.95 (11.1)	1.59 (22.3)	
0.5	1.78 (10.3)	3.05 (20.6)	

Q/A = 100 ft/sec

K	NOMINAL $4f\frac{L}{D}$		*(ACTUAL)
	10	20	
0.2	2.06 (9.7)	3.66 (19.4)	
0.5	4.04 (8.6)	7.22 (17.1)	

* Actual 4fL/D values based on loading plus evaporation
at t_{fill}.
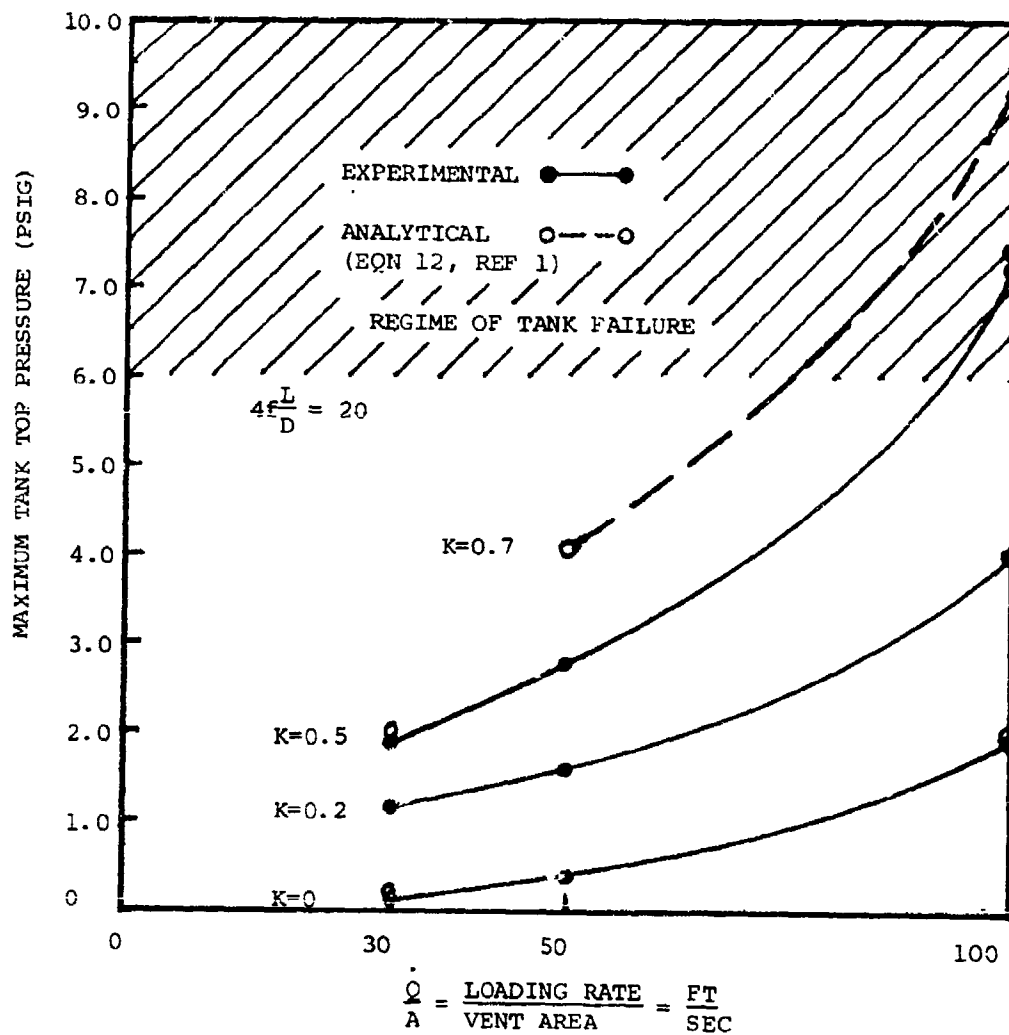
FIGURE 12 - MAXIMUM TANK TOP PRESSURE vs TRANSFER RATE
(4fD/L=20)

34
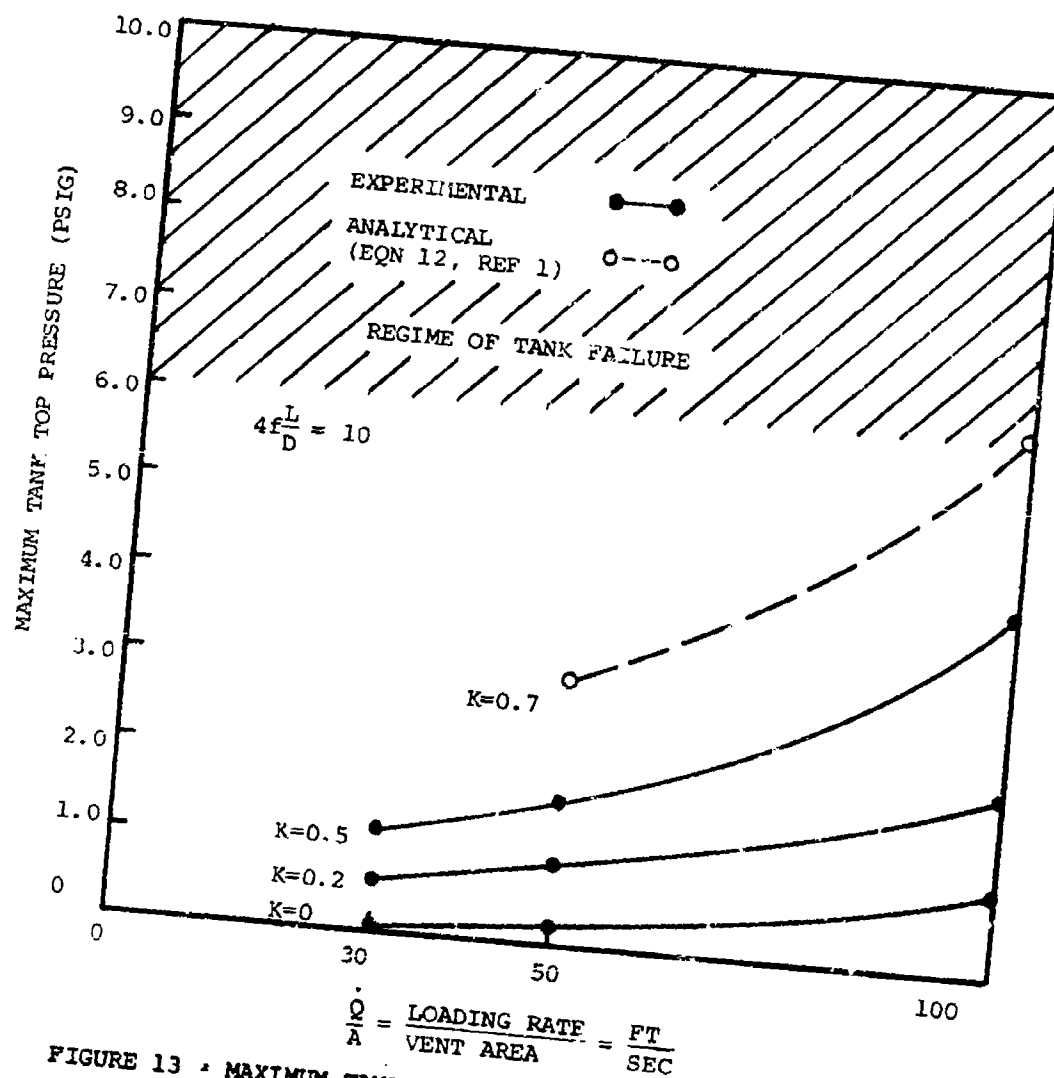
FIGURE 13 - MAXIMUM TANK TOP PRESSURE vs TRANSFER RATE
(4fD/L=10)

35

V. EVALUATION OF TANK PRESSURE UNLOADING CARGO

A. Analytical Formulation

The following formulation describing tank top pressure while un-loading cargo was arrived at in a manner similar to that employed by Wilson and Raj[1] in developing an analytical model describing tank pressure as a function of time when loading cargo. The effect of cargo evaporation on the rate of pressure rise was not considered since any cargo evaporation would tend to reduce the magnitude of negative gage pressure created inside the tank.

A mass balance on the vapor/air mixture in the tank is first written:

$$\frac{dM}{dt} = -\dot{M}_v \qquad (9)$$

$\underbrace{\hspace{2cm}}$ Rate of change of air mass in the tank

$\underbrace{\hspace{2cm}}$ Mass rate of venting

The left hand side is developed as follows. The mass in the tank for a compressible gas can be expressed as:

$$M = \rho V = \rho_a V_T \left(\frac{\rho V}{\rho_a V_T} \right) \qquad (10)$$

where:

ρ = density of vapor air mixture

ρ_a = density of gas or air at initial condition

V = volume of vapor space at any instant of time

V_T = total tank volume

Letting V_i be the initial tank volume not occupied by liquid and t_e be the characteristic unloading time ($t_e = (V_T - V_i)/\dot{Q}$), then:

36

$$\frac{V}{V_T} = \frac{V_i + \dot{Q}t}{V_i + \dot{Q}t_e} \tag{11}$$

Additionally, for an isothermal gas, $\rho/\rho_a = p/p_a$ and equation (10) can be expressed as:

$$M = \rho_a \, (V_i + \dot{Q}t_e)(p/p_a) \left(\frac{V_i + \dot{Q}t}{V_i + \dot{Q}t_e} \right) \tag{12}$$

The venting rate is now related to the pressure rise. Employing equation (6.42) on page 182 from Shapiro,[4] a relationship between the pressures on the upstream and downstream side of the vent can be developed. Doing this we get:

$$p_a^{\,2} - p^2 = \left(\frac{\dot{M}_v}{A} \right)^2 RT \left[2 \;\; (p_a/p) \;\; + 4f\frac{L}{D} \right] \tag{13}$$

By solving equation (13) for $\dot{M}_v$, differentiating equation (12) and substituting equations (12) and (13) into equation (9), and then dividing both sides of the resulting equation by $\dot{Q}\rho_a$, the following expression is obtained:

$$\left(\frac{V_i + \dot{Q}t}{\dot{Q}t_e} \right) \frac{d(p/p_a)}{d(t/t_e)} = - \frac{p}{p_a} - \frac{\left[1 - (p/p_a)^2 \right]^{\frac{1}{2}} \sqrt{RT}}{(\dot{Q}/A) \left[4fL/D + 2 \; \ln(p_a/p) \right]^{\frac{1}{2}}} \tag{14}$$

Equation (14) is subject to the initial condition $p/p_a = 1$ at $t = 0$ and can be numerically integrated. The key parameters of equation (14) are $\dot{Q}/A$, $4f \, L/D$, t/t_e and V_i. A useful and more easily used solution to equation (14) can be arrived at by assuming $d(p/p_a)/d(t/t_e) = 0$. The rationale for equating the left side of equation (14) to zero is based on experimental results, where it was observed that the vacuum magnitude

37

in the tank would approach a finite value (depending on pumping rate and vent restriction) and remain constant within the accuracy of the Data Acquisition System (DAS), e.g., $d(p/p_a)/d(t/t_e)=0$. Thus equating the left side of equation (14) to zero results in:

$$\frac{p}{p_a} = \left[\frac{RT}{RT + (\dot{Q}/A)^2 \left[2 \ln(p_a/p) + 4fL/D \right]} \right]^{\frac{1}{2}} \qquad (15)$$

Equation (15) cannot be solved directly, but must be iterated to arrive at a solution. Solving equation (15) for p/p_a without the term $2 \ln(p_a/p)$ in the denominator and then using this first step value of p/p_a in the complete expression and resolving for p/p_a, hastens the iterative process. Convergence is rapid since $2 \ln(p_a/p)$ is small compared to $4f L/D$. Thus, equation (15) presents a simplified expression for arriving at the maximum vacuum to be expected for any combination of loading rate and vent restriction. Additionally, this expression provides a conservative worst case for cargo offloading in that cargo evaporation, which would tend to decrease the maximum tank vacuum attained, was neglected in the problem formulation.

B. Experimental Results Unloading Cargo

In order to compare the pressure-time histories for various vent systems and unloading rates, the following cargo transfer parameters were chosen:

    $4f L/D = 10, 20,$ and 35

    $\dot{Q}/A = 30, 50, 100$ and 150 ft/sec.

As mentioned previously in the analytical formulation, the effect of cargo evaporation was neglected, ($K=0$), providing a conservative worst

38

case since any cargo evaporation will compensate for a portion of the vacuum buildup. Additionally, the unloading evaluations were performed with the tank being partially full ($V_i=0$, 1/2, 1/3, etc.) to assess the effect of this parameter on the rate of vacuum rise.

Figure 14 shows the effect the initial amount of cargo in the tank has on the rate of vacuum rise. From Figure 14 it can be seen that the smaller the vapor space is when offloading is begun, the more rapid is the vacuum buildup, and experimental results also indicate that the initial cargo volume does not affect the maximum vacuum attained (within the accuracy of the DAS and for the range of parameters explored). Table 4 presents the results obtained from the experimental evaluation of cargo unloading in the form of the maximum vacuum attained for the $\dot{Q}/A$ and 4fL/D values examined. Also included in Table 4 are the maximum vacuums as predicted by the simplified analytical model, equation (15). One will note that the correlation between the analytical and experimental results is quite good and most certainly within the bounds of experimental error.

Figure 15 shows the relationship between cargo unloading rate ($\dot{Q}/A$) and maximum vacuum attained in the tank for various vent system restrictions (4f L/D) as predicted by equation (15). It was noted during the experiments that a buckling of the tank top can occur as a result of the combined effects of the tank vacuum created by unloading cargo and the geometry of the tank top, especially when the tank top is cambered.

This instability may occur at a vacuum which is less (in absolute magnitude) than the positive pressure required to cause a yielding type tank failure. The combinations of tank internal vacuum and tank top

39
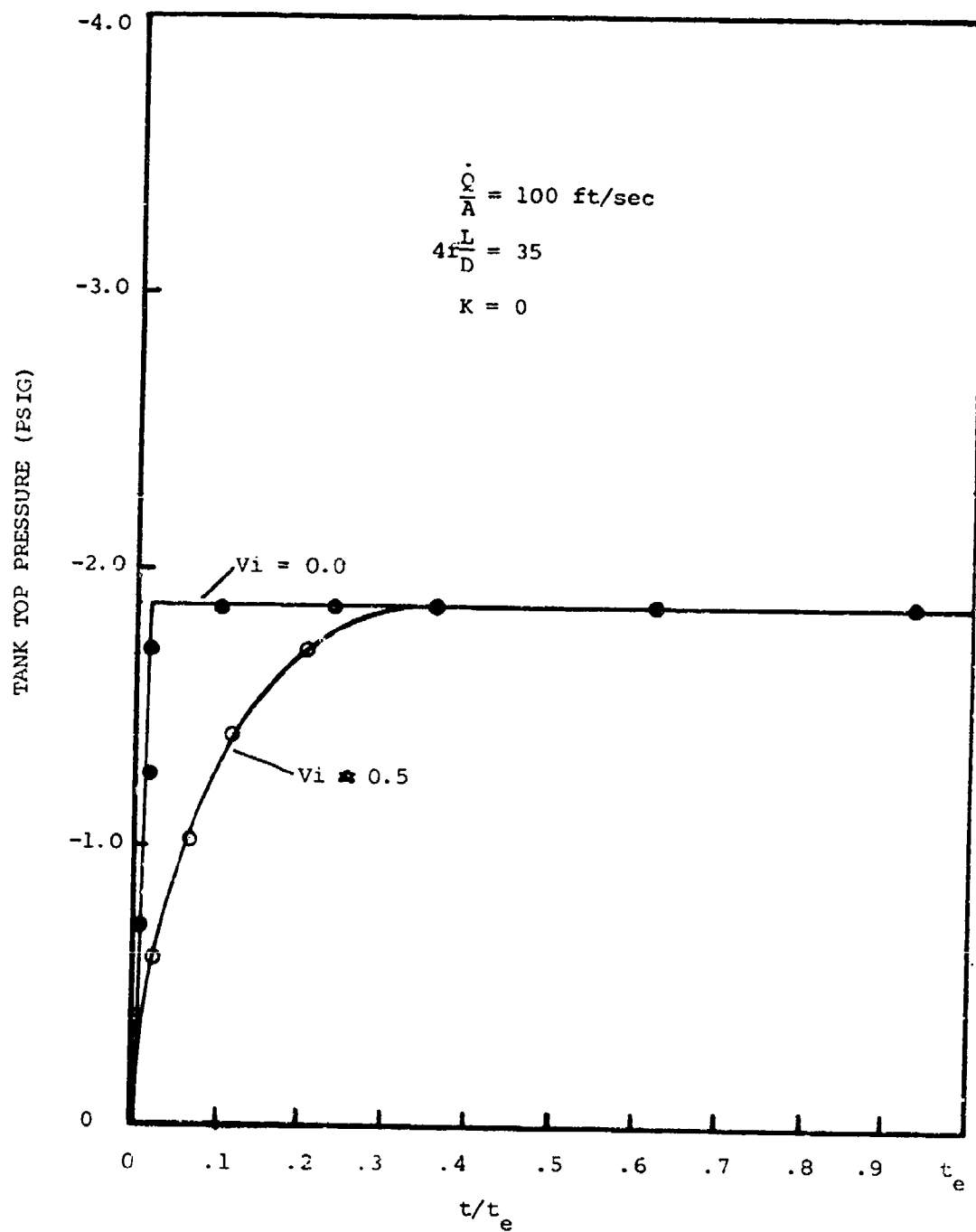
FIGURE 14 - EFFECT OF INITIAL LIQUID VOLUME ON PRESSURE --
TIME HISTORY UNLOADING CARGO FOR EXPERIMENTAL
MODEL

40

TABLE 4

ANALYTICAL AND EXPERIMENTAL
MAXIMUM VACUUM UNLOADING CARGO

$$P_{min} \text{ (psig)}$$

$\dfrac{\dot{Q}}{A}$		NOMINAL $4f\dfrac{L}{D}$		
		*(ACTUAL)	*(ACTUAL)	*(ACTUAL)
(ft/sec)		10	20	35
30	Experimental	-.09 (12.6)	-.18 (25.2)	-.31 (44.2)
	Analytical	-.09	-.18	-.30
50	Experimental	-.23 (11.4)	-.44 (22.8)	-.77 (41.0)
	Analytical	-.25	-.45	-.78
100	Experimental	-.76 (10.0)	-1.38 (19.5)	-2.19 (34.0)
	Analytical	-.84	-1.35	-2.18
150	Experimental	-1.47 (9.2)	-2.54 (18.1)	**
	Analytical	-1.65	-2.53	

* Actual $4f\dfrac{L}{D}$ value used experimentally and for analytical calculations (see Appendix A).

** Unloading rate and vent restriction combination produce choked flow.

41
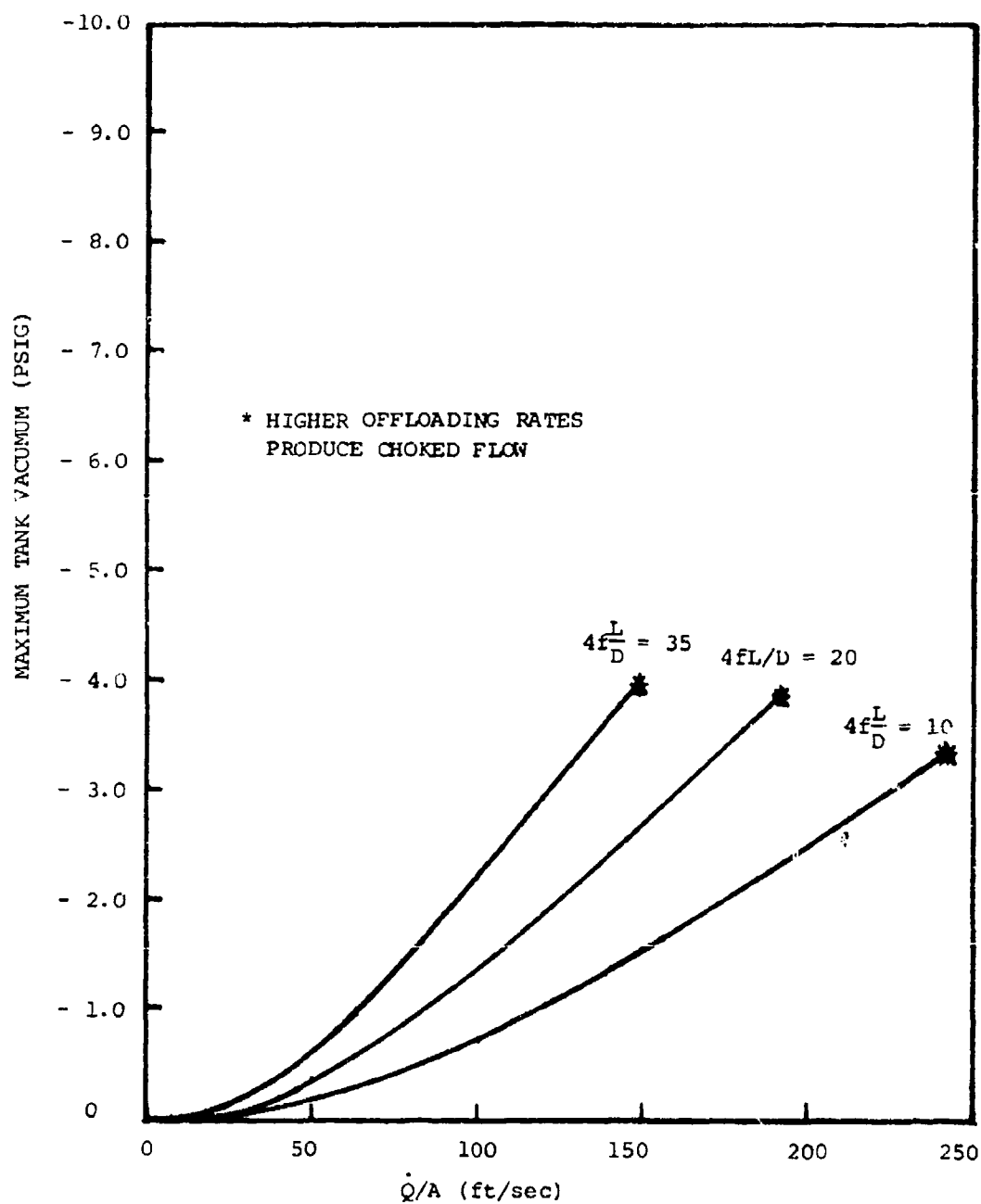
FIGURE 15 - MAXIMUM TANK VACUUM vs TRANSFER RATE FOR
OFFLOADING NON VOLATILE CARGO FOR ANALYTICAL
MODEL (EQUATION 15)

42

geometric configuration which would cause the tank and/or deck to collapse inward are beyond the confines of this investigation, but should be considered when establishing safe unloading rates, especially for tanks with camber.

A. Evaluation of Parameters

Equation (4) shows the rate of tank top pressure rise during liquid overfill to be a function of the following parameters:

B = tank volume of expansion coefficient by pressure $(\frac{1}{V_T} \frac{dV}{dp})$

V_T/A = ratio of tank volume to vent area

$\dot{Q}/A$ = ratio of loading rate to vent area

χ = compressibility of liquid $(\frac{1}{\rho} \frac{d\rho}{dp})$

U = mean velocity of liquid in the vent pipe

The volume of expansion coefficient for the model tank is 0.000388 psi^{-1} which is within the range of values for typical prototype tanks 0.001 to 0.00001 psi^{-1}) [1]. The compressibility of the liquid being pumped into the tank (water) is 0.0000033 psi^{-1} and therefore is generally less than the tank bulk modulus; hence the accomodation of pressure rise in the tank is usually governed by the tank expansion.   The relationship between the model cargo compressibility and the model tank bulk modulus is not unlike that to be expected from a prototype situation, in that for the case of a full scale tank being overfilled, the rate of pressure rise would be governed by the tank bulk modulus more so than the compressibility of the cargo ($B \gg \chi$). The loading rate was held constant during each test, and loading rates ($\dot{Q}/A$) of 30, 50, and 100 ft/sec were examined.   The ratio of tank volume to vent area (V_T/A) for the experimental model is 40,196 ft and is in the range of typical V_T/A tank volume to vent area ratios for most barges (V_T/A barges = 14,000 to 224,000 ft).   Thus, the overfill model represents a barge tank during liquid overfill and has a pressure-

44

time history which corresponds to a barge with the same parameters. Figure 16 shows the experimental results of the overfill cases run for loading rates of 30, 50, and 100 ft/sec. Also included in the figure is the expected regime of tank failure for vessels of this type. For this case, tank failure can be expected within approximately 10 seconds from the time the tank becomes liquid full. The tank flexibility plays an important role in helping to delay the pressure buildup. This phenomenon is due to the fact that initially the outflow velocity of the liquid is appreciably less than the inflow velocity, and considerable liquid accumulates in the tank due to tank flexing (e.g. an infinitely stiff tank, $B=0$, would result in an infinitely rapid pressure rise). Since the pressure-time histories generated analytically and experimentally had different parameter values, a direct comparison of results could not be made. However, both experimental and analytical models indicate that tank failure will occur a short time after the tank becomes liquid full (generally less than one minute).

Equation (6) is a steady incompressible flow formulation of flow through the vent system and defines the liquid efflux velocity at which cargo can pass indefinitely through the vent system. For a typical vent system and tank configuration with 4f L/D=10, a vent pipe rise, H = 8ft and an allowable pressure P_{max} = 6 psig, the maximum loading rate to vent cross sectional area is about 6 ft/sec. Thus, for loading rates higher than this (typically higher rates are employed), tank failure will occur in a relatively short time if overfill is allowed to occur. Because of this, some type of device to protect the tank should be employed.
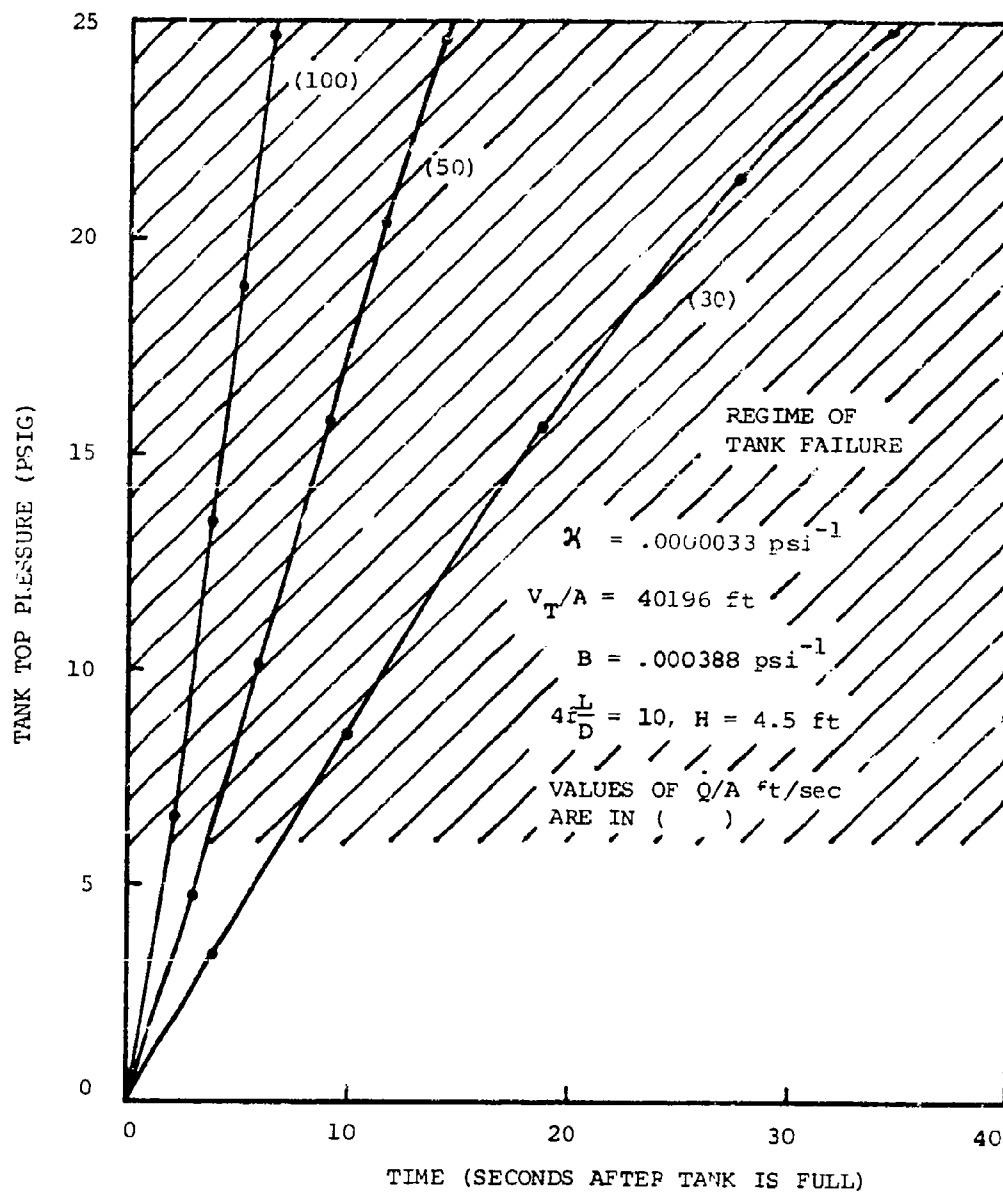
FIGURE 16 - OVERFILL PRESSURE - TIME HISTORIES
FOR EXPERIMENTAL MODEL

46

B.   Pres   e History When Vent is Blocked

The effect of a blocked vent or stuck P-V valve on the tank pressure buildup can best be examined by looking at two separate cases. The first would be when the vent becomes blocked after the tank is liquid full and the second would be to examine the effect of vent blockage before the tank is full. The blocked vent was modeled by installing a ball valve in the model vent and closing it off at the appropriate time (e.g. either before or after overfill).

For the case of a blocked vent after overfill had commenced. the tank was allowed to overfill and reach a steady state flow condition (a large diameter vent pipe was employed and the resulting steady state pressure was less than 1 psig) and the ball valve was then closed, with time beginning after the valve was closed. Even though the tank was allowed to become liquid full, a small amount of trapped air remained in the tank due to the tank top geometry and the intrusion of the vent pipe fixture back into the tank. The effect of the trapped air on the rate of pressure rise in the tank was examined by running the blocked vent cases with the tank physically oriented in two ways as is depicted in Figure 17.

The effect that the amount of trapped air had on the rate of pressure rise in the tank can be observed in Figure 18 where the experimental pressure time histories for both barrel orientations are shown along with the analytical pressure history for the same case with no trapped air. This discrepancy between the results is due to the entrapped air in the tank and can be best explained by considering the stiffness of the tank and the compressibility of the trapped air as two springs in series. In this case though, one spring stiffness (the air) is initially much

47

10 in^3 trapped air

TILTED CONFIGURATION

350 in^3 of trapped air

UPRIGHT CONFIGURATION
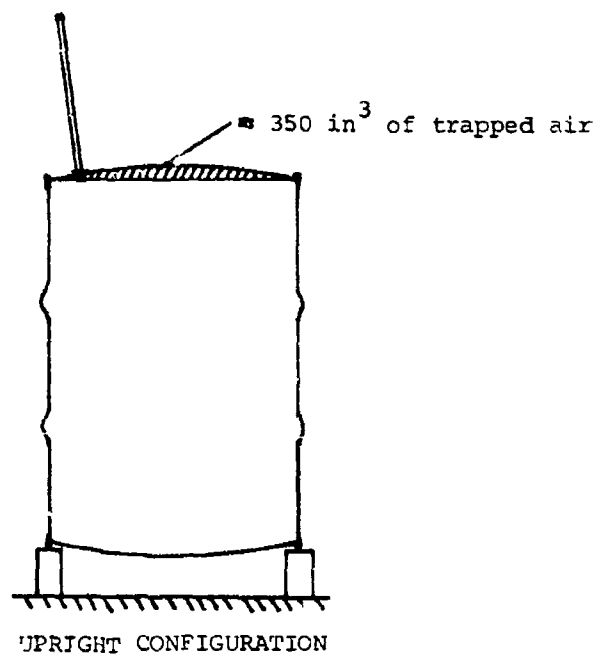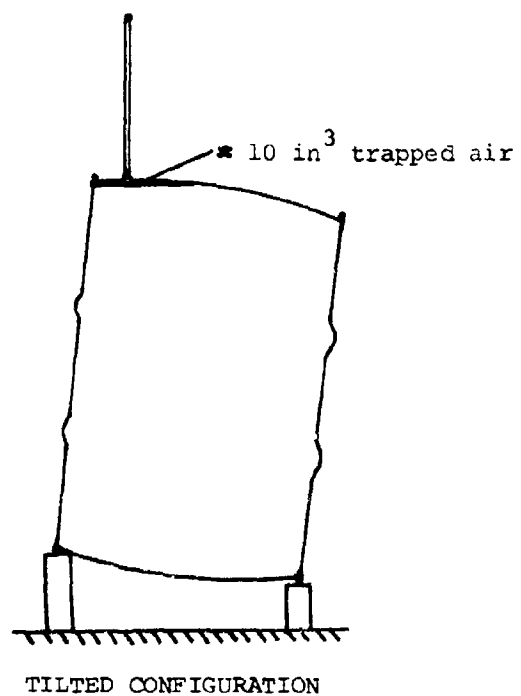
FIGURE 17 - EFFECT OF TANK ORIENTATION ON THE
AMOUNT OF TRAPPED AIR IN THE TANK

48
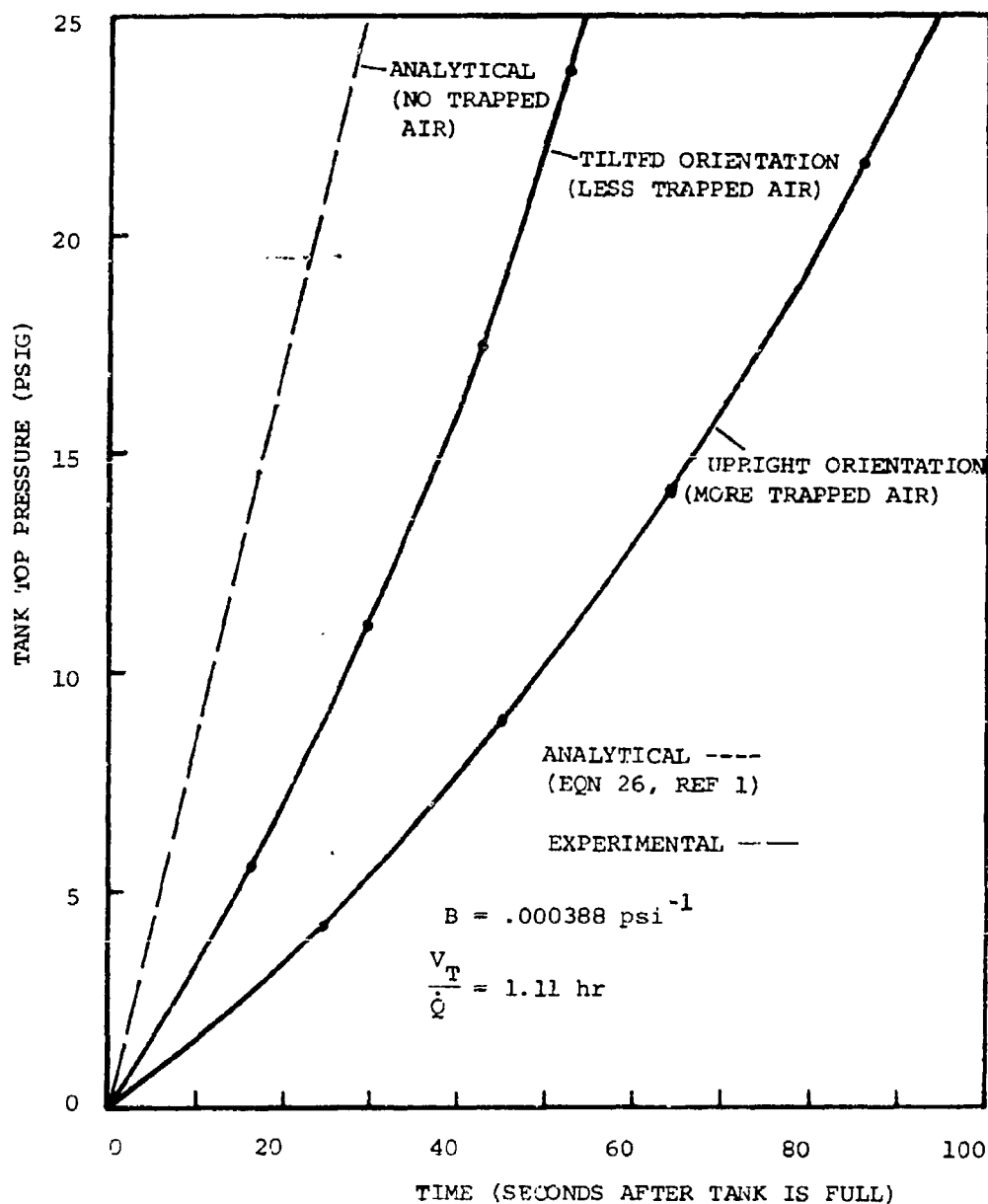
FIGURE 18 - EXPERIMENTAL AND ANALYTICAL PRESSURE - TIME
HISTORIES FOR A BLOCKED VENT

49

softer and has a stiffness which is changing rapidly (becoming stiffer) with respect to the other (the tank) as the pressure inside the tank is increasing. The relationship between stiffness and bulk modulus is that a stiffer object would have a smaller bulk modulus. When the stiffness of the air becomes greater than that of the tank structure itself, the stiffness of the tank would then begin to govern the pressure rise in the tank and approach the rate of pressure rise predicted by equation (5) which does not consider air trapped in the tank.

Then, by running the blocked vent case with the tank in a tilted configuration (little trapped air), a pressure-time history is attained which more closely resembles that predicted by the analytical model than that obtained by running the test with the tank in a upright configu tion. That is, the slope of the tilted configuration p vs. t curve more rapidly approaches the slope of the analytical curve than does the p vs. t curve of the vertical configuration. Further, it is felt that both curves (tilted and vertical configurations) would have eventually attained the slope of the anlytical model had the test not been terminated at 25 psig for reasons of safety.

Figures 19 and 20 show experimental pressure-time histories for two vent restrictions (4f L/D = 10, ∞)and two loading rates ($\dot{Q}/A$ = 100 and 23 ft/sec) and analytical pressure-time histories for the infinite vent restric tion or blocked vent case. One will note from Figures 19 and 20 that the difference in the pressure-time history for a finite (4f L/D = 10) and infinite vent restriction (blocked vent) is relatively small in the early stages of overfill up to the regime of tank failure. Thus, the blocked

50
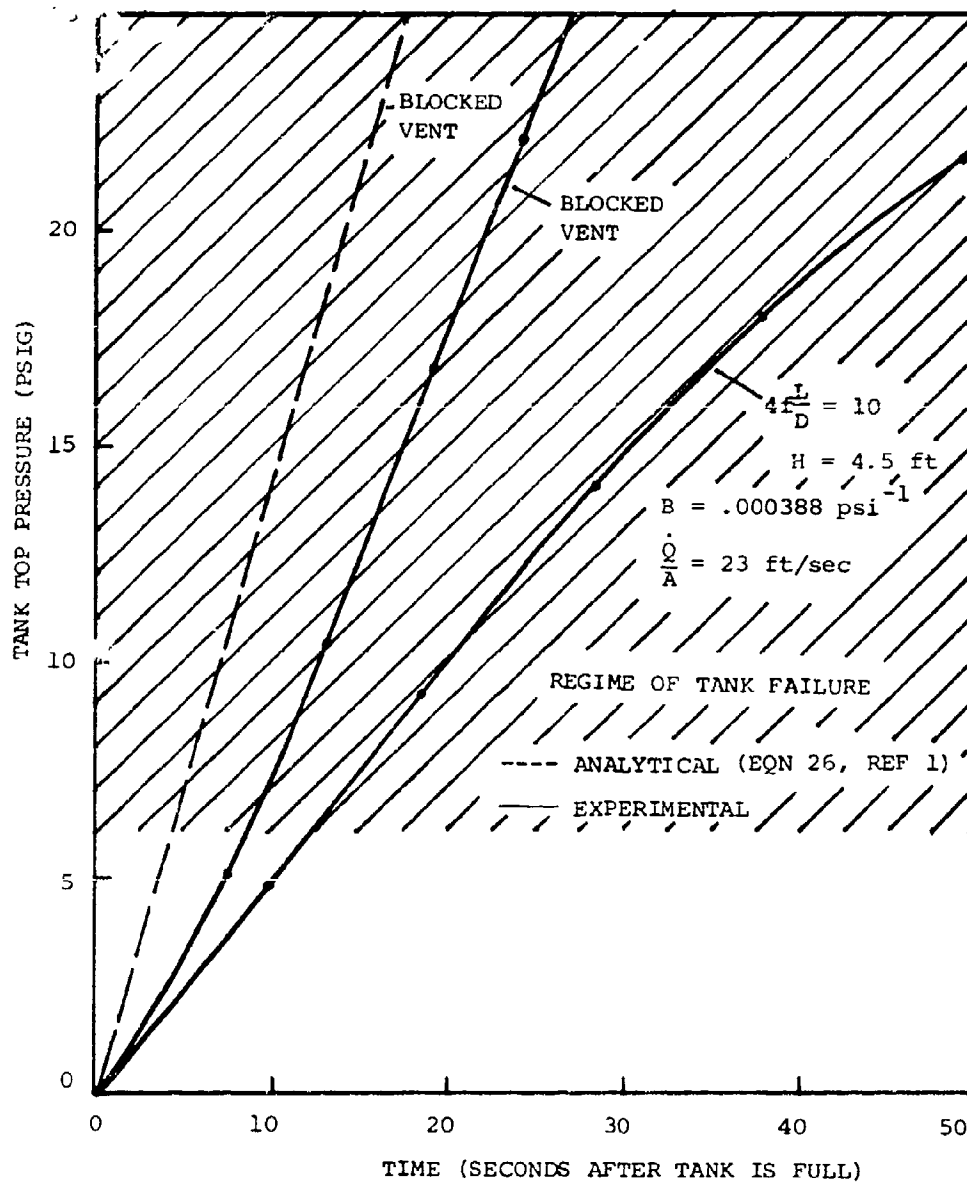
FIGURE 19 - EFFECT OF VENT RESTRICTION ON PRESSURE - TIME HISTORY
($\dot{Q}/A$ = 23 ft/sec)

51
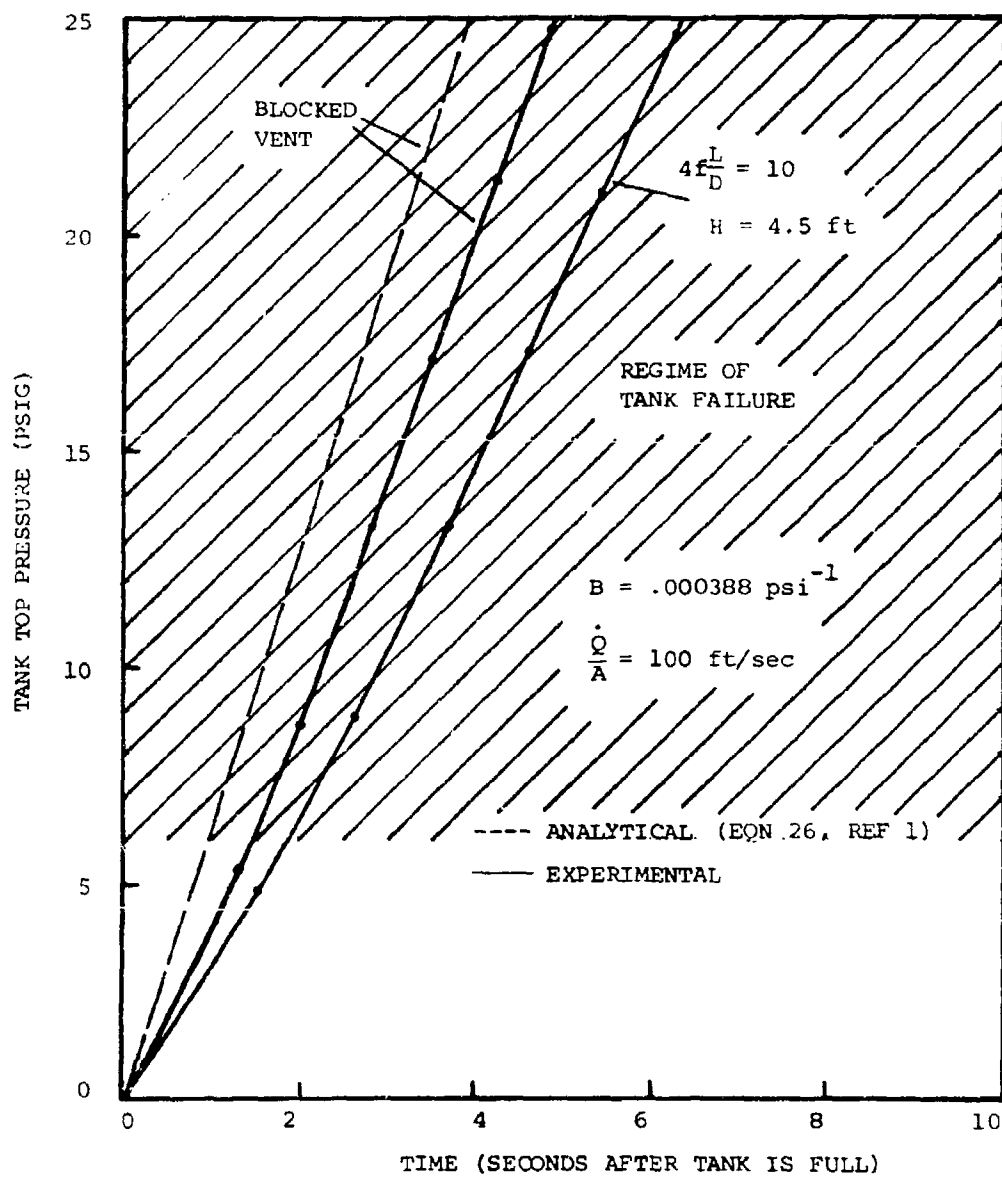
FIGURE 20 - EFFECT OF VENT RESTRICTION ON PRESSURE - TIME HISTORY
($\dot{Q}/A$ = 100 ft/sec)

52

vent case provides an easily employed, although conservative, worst case solution for estimating the time to tank failure once overfill begins.

The second case to consider is that of a vent being blocked before the tank becomes liquid full (e.g. a stuck PV valve). This situation was modeled experimentally by closing the ball valve in the vent system before the tank was liquid full. Figure 21 shows an experimentally derived pressure-time history arrived at in the manner just described. The ball valve was closed with the tank 60% full (simulating a relief valve incapable of relieving tank pressure) employing a simulated transfer rate $\dot{Q}/A$ of 23 ft/sec.

The phenomena occurring is the same as that described previously when there was air trapped in the tank during liquid overfill, only now because of the large volume of air trapped in the tank, the bulk modulus of the trapped air is not changing as rapidly as before and thus the pressure rise is not as rapid. As one can see from Figure 21, where the tank pressure is plotted aginst the fraction of total fill time, the pressure rise in the tank approaches the failure regime of the tank long before the tank becomes liquid full. Thus, the employment of warning devices based on the tank liquid level would be ineffective against this situation. An automatic shutoff mechanism triggered by pressure would be needed to provide protection against this occurrence.

53
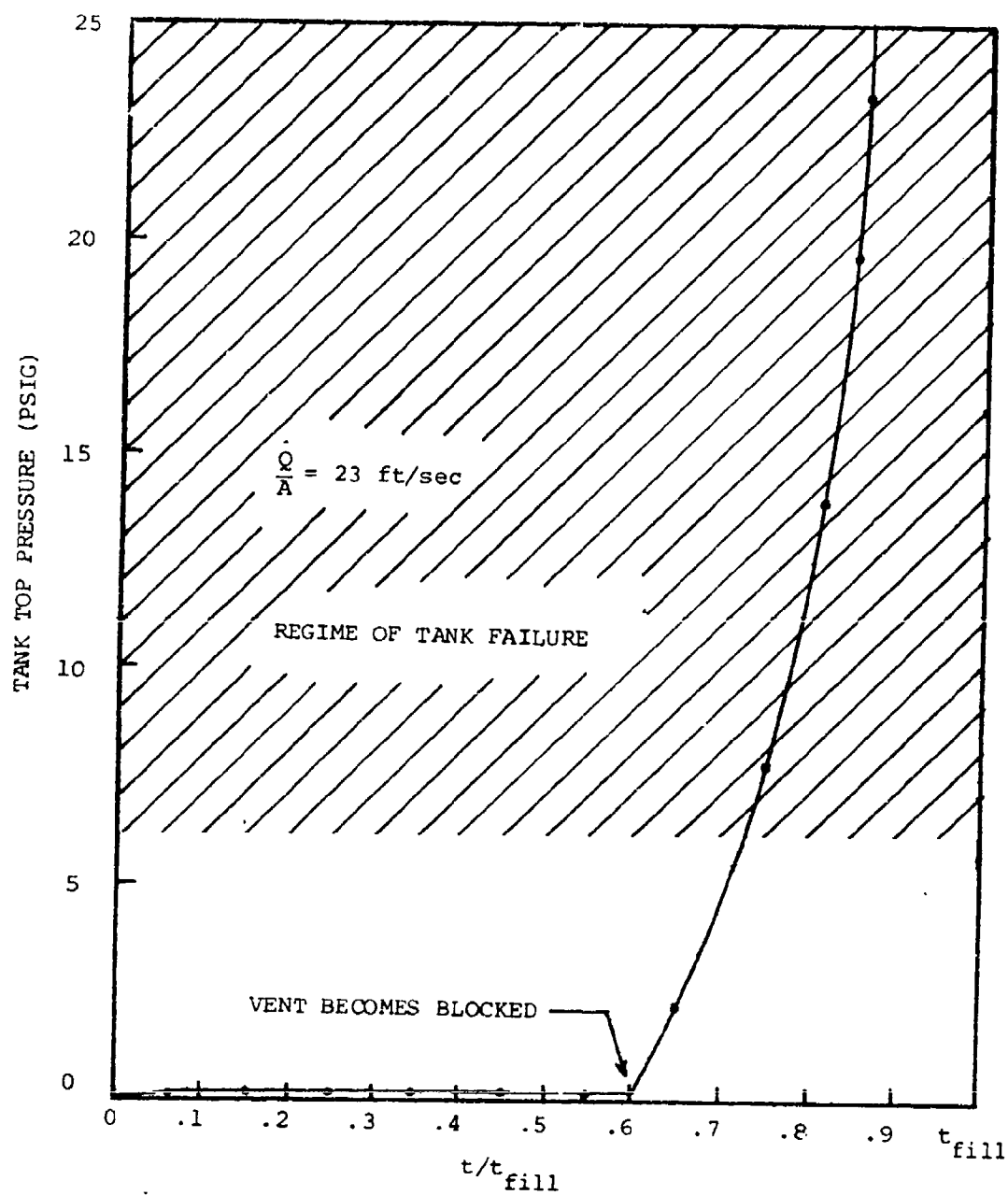
FIGURE 21 - EFFECT OF BLOCKED VENT BEFORE TANK BECOMES LIQUID FULL FOR EXPERIMENTAL MODEL

54

VII. SUMMARY OF FINDINGS

A. Normal Transfer of Cargo

1. The analytical model of cargo loading with and without cargo evaporation, equation (2), as developed by Wilson and Raj[1] predicts the pressure-time history of a cargo tank being loaded within the constraints of the assumptions made by the analytical model for evaporation.

2. An analytical model for cargo offloading, equation (14), can be employed to predict pressure-time histories for a cargo tank being off-loaded. This formulation is conservative for volatile cargoes. A simplified expression, equation (15), was derived from equation (14) to predict the maximum vacuum attained offloading cargo, and has been validated through scale model tests.

3. From the analyses and experimental results, the following conclusions were reached for non-volatile cargoes:

• The maximum tank pressure for loading non-volatile 'cargo can be calculated using the simplified expression for loading cargo, equation (8).

• The maximum tank vacuum occurring when offloading cargo can be calculated using the simplified expression for offloading cargo, equation (15).

• The maximum tank pressures resulting during the loading of non-volatile cargoes are small compared to calculated tank failure pressures for typical loading rates and vent restrictions ($\dot{Q}/A = 30$ ft/sec and $4f L/D = 10$).

• The absolute value of the maximum vacuum attained unloading cargo is less than the absolute value of the maximum tank top pressure attained

55

when loading cargo, indicating the danger of tank failure defined as reaching tank material yield to be less than when loading cargo, but the possibility of tank top buckling at a lower pressure (due to tank top geometry conforming to that of a cambered deck) when unloading cargo should also be considered.

· For high loading rates and vent restrictions the maximum tank top pressure changes rapidly with small changes in loading rate, indicating the danger in employing these higher rates.

4. For normal vent systems, cargo volatilities, and cargo loading rates, it appears that volatile cargoes can be loaded with an adequate safety factor for tank pressure rise (subject to the assumptions of the evaporation model).

B. Liquid Overfill

The steady incompressible flow formulation for flow through the vent system as given in equation (6)

$$\dot{Q}/A = U = \left[\frac{p - p_a - \rho g H}{\frac{1}{2} \rho [4f \ L/D + 1]} \right]^{\frac{1}{2}}$$

can be used to determine the maximum allowable loading rate to vent cross section area ratio ($\dot{Q}/A = U$) at which cargo could safely pass indefinitely through the vent system. For a tank failure pressure of 6 psig with a vent restriction of 10 and a vertical rise of 8 ft, the maximum $\dot{Q}/A$ ratio would be approximately 6 ft/sec. For a higher rate of loading or a smaller vent system capacity, tank failure will occur within a relatively short time after the tank becomes liquid full.

The effect of trapped air in the tank has the net effect of decreasing the rate of pressure rise in the tank, but not to the extent of diminishing

the danger presented by liquid overfill. Tank flexure plays a similar
role in relieving overfill pressure, with a stiffer tank reaching
failure pressures more rapidly than a more flexible one. Further, with
these considerations, it still appears that tank failure will occur
within about 30 seconds after the tank becomes liquid full, for normal
combinations of loading rate and vent restriction.

Thus, it appears that some type of automatic shut-off mechanism
triggered by pressure to shut off the liquid flowing into the tank must
be provided to protect the tank. Another possibility would be a
pressure triggered hatch cut into the tank top at the deck level which
has sufficient area to allow liquid overflow without any dangerous
pressure buildup. In addition, any system employed should have high
level alarms to warn the operator of the impending danger.

VIII. APPLICATION TO VENT SYSTEM EVALUATION AND DESIGN

One can evaluate the adequacy of an existing vent system for avoiding overpressure in an individual tank by employing the following steps:

1. Calculate the characteristic venting velocity $\dot{Q}/A$ (ft/sec) for the tank in question by determining the loading rate $\dot{Q}$ (ft^3/sec) from the loading rate and number of tanks to be loaded simultaneously and dividing by the cross-sectional area A(ft^2) of the vent pipe(s) coming out of the tanks.

2. Calculate the effective length to diameter ratio L/D of the vent system by first dividing each pipe length employed in the vent system by its respective diameter and then summing. Then add in all the equivalent L/D ratios for all bends, elbows, tees, valves, flame arrestors and the entrance loss associated with each vent pipe. These values can be found in most handbooks or References 1, 5 or 6.

3. The maximum expected tank pressure loading cargo can be determined using Table 5 and the values of $\dot{Q}/A$ and L/D determined in steps 1 and 2. Table 5 was developed by ADL using equation (2) with a high evaporation rate (K = 0.7), which it is felt provides some factor of safety.

4. The maximum expected vacuum created in the tank when offloading cargo can be determined using equation (15) and the values of $\dot{Q}/A$ and L/D determined in steps (1) and (2) (assume 4f = .02 and RT = 900,000 ft^2/sec^2).

5. The maximum pressure during cargo overfill can be arrived at by first determining the height of the vertical portion of the vent pipe H and then using equation (6) and the values of H, $\dot{Q}/A$ and 4f L/D previously determined.

58

TABLE 5

MAXIMUM TANK PRESSURES (PSIG) FOR GIVEN VALUES OF VENT SYSTEM L/D and $\dot{Q}/A$ (BASED ON f = .005) K = 0.7

(FROM REFERENCE 1)

Q/A (FT/SEC)

L/D	10	15	20	25	30	40	50	60	80	100	150	200
400							2.7	3.2	4.2	5.3		
600							3.2	3.8	5.1			
800						3.0	3.	4.4	5.9			
1000						3.3	4.1	4.9				
1200					2.8	3.6	4.4	5.4				
1600					3.1	4.1	5.1					
2000				3.0	3.5	4.6	5.8					
2400				3.2	3.8	5.0						
3200			3.0	3.6	4.3	5.9						
4000			3.3	4.0	4.8							
6000	2.2	3.0	4.0	4.9	6.0							
8000	2.5	3.5	4.6	5.8								
10000	2.7	3.8	5.1									
12000	2.9	4.2	5.6									
16000	3.3	4.8										
20000	3.6	5.4										
24000	3.9	6.0										
32000	4.5											
40000	5.1											

Tank pressure less than 3 psi

Tank pressure greater than 6 psi - hazardous for most vessels

6. Compare the expected pressures arrived at in steps 3 through 5 with the expected tank failure pressure. Tank failure pressure can be obtained from a structural analysis of the tank in question or in lieu of such an anlysis the ADL value of 6 psig may be employed.

Based on estimates of tank failure pressure and typical vent restrictions (6psig and 4f L/D = 3 to 10), experimental results indicate that typical vent systems in use today have an adequate capacity for gas venting but an inadequate capacity for liquid overfill. Further, any vent system designed to facilitate liquid overfill would be extremely overdesigned for normal gas venting. Thus, it appears that a practical approach to vent system design would be to design the vent system to accomodate normal gas venting with an adequate safety factor in addition to incorporating preventative measures in the tank/vent system to avoid or relieve the occurence of liquid overfill.

Units

A   = cross sectional flow area ft^2

B   = coefficient of volume expansion of tank by pressure psi^{-1}

     $= \frac{1}{V_T} (\frac{dV}{dp})$

f   = fanning friction factor in the vent pipe

g   = acceleration due to gravity ft/sec^2

H   = height of the vertical portion of the vent pipe   ft

K   = ratio of evaporation rate to the loading rate   -
       taken at t_{fill}

L   = effective length of vent pipe   ft

L/D = effective length to diameter ratio   -

$\dot{M}_v$ = rate of mass efflux through the vent   lbm/sec

$\dot{M}_c$ = characteristic mass efflux rate of air $= \rho_a \dot{Q}$ lbm/sec

$\dot{M}_{vap}$ = rate of vapor mass addition to the ullage by   lbm/sec
       evaporation

M   = mass of liquid in the tank at any time   lbm

$\dot{M}_i$ = rate of mass inflow (liquid filling rate)   lbm/sec

p   = pressure inside the tank (at the top of the tank)   psi

p_a = atmospheric pressure   psi

P   = gauge pressure inside the tank   psig

$\dot{Q}$ = volumetric liquid filling rate ft^3/sec

R   = gas constant = 1698.7 $ft^2/sec^2/°R$

Re   = Reynolds number for flow in the pipe $= \frac{UD}{\nu}$ -

t   = time   sec

t_{fill} = characteristic tank filling time (volume of tank   sec
       divided by loading rate)

61

			Units
T	= temperature		R
U	= mean velocity of liquid in the vent pipe		ft/sec
V	= tank volume not occupied by liquid at any instant of time		ft^3
V_i	= initial tank volume not occupied by liquid		ft^3
V_T	= total tank volume		ft^3
ϵ	= vent pipe roughness		ft
χ	= compressibility of liquid = $\frac{1}{\rho}\frac{d\rho}{dp}$		psi^{-1}
ν	= kinematic viscosity		ft^2/sec
ρ	= density of liquid		lbm/ft^3
ρ_a	= density of gas		lbm/ft^3
ρ_{vap}	= density of pure vapor		lbm/ft^3

REFERENCES

1. Wilson, R. P., Jr. and Raj, P. K. P., Vent System and Loading Criteria For Avoiding Tank Overpressurization, Department of Transportation Report No. CG-D-59-77, September 1977.

2. Hovanesian, J. and Y. Y. Hung, Moiré Contour-Sum Contour-Difference, and Vibration Analysis of Arbitrary Objects, Applied Optics, Vol. 10, No. 12, December 1971.

3. Meadows, D. M., W. O. Johnson and J. B. Allen, Generation of Surface Contours by Moire Patterns, Applied Optics, Vo. 9, No. 4, April 1970.

4. Shapiro, A. H., The Dynamics and Thermodynamics of Compressible Fluid Flow, Vol. I, P. 83, Ronald Press, New York (1953).

5. Baumeister, (Editor), Marks' Handbook for Mechanical Engineers, 7th Edition, McGraw-Hill, New York, (1967).

6. Flow of Fluids Through Valves, Fittings, and Pipe, Crane Co., Technical Paper No. 410, Chicago (1969).

7. Streeter, V. L., Fluid Mechanics, McGraw-Hill, 4th Edition, New York (1966).

APPENDIX A

DETERMINATION OF MODEL VENT PIPE ROUGHNESS

Accurate determination of the model vent pipe roughness was necessary
to accurately model the vent system restriction, 4f L/D. Since a model
vent pipe of diameter D could be cut to any length L, accurate modeling of
the vent restriction would be directly related to the establishment of the
pipe Fanning friction factor **f**. The friction factor for a particular
pipe is a direct function of Reynolds number Re, and pipe relative roughness
ϵ/D, where the two parameters can be related on a Moody diagram. In a
typical pipe flow calculation all quantities except, 4f, can be measured.
Thus, by conducting a pipe flow experiment using the model vent pipe, one
would be able to calculate the friction factor,4f,directly for the par-
ticular Reynolds number at which the test was run. Knowing these two
quantities and employing a Moody diagram, one would then be able to de-
termine the model vent pipe relative roughness and enable one to model the
vent restriction 4f L/D for any Reynolds number (e.g. gas efflux velocity
through the vent system).

An attempt was made to arrive at the vent pipe roughness by measuring
the head loss resulting with water flowing through the model vent pipe.
But because of the inability to attain a steady state of flow and the lack
of consistency of results, this method of roughness determination was
abandoned in favor of the following method. A known length of model vent
pipe was installed in the tank top and air was then pumped through a flow-
meter at a constant rate venting to the ambient. The pressure on the
upstream side of the vent pipe was monitored by a pressure transducer

65

located on the tank top. A sketch of the pipe roughness experimental
test setup can be found in Figure A-1.

By writing an energy balance between points 1 and 2 and accounting
for all losses the following equation results:

$$4f = \left[\left(\frac{P_1}{\gamma} - L\right)\left(\frac{2g A^2}{\dot{Q}^2}\right) - \left(1 + C_c\right)\right]\frac{D}{L} \qquad \text{(A1)}$$

where C_c is the orifice contraction coefficient, accounting for the losses
of the connecting fixture at the vent pipe orifice. Equation (A 1) con-
tains two unknowns, 4f and C_c. By running the experiment with two lengths
of pipe, the resulting equations could be solved simultaneously for 4f and
C_c.

Results of the roughness evaluations run on the pipe sections to be
used in the venting model are shown in Figure A-2 as points on a Moody
diagram. Taking the average of the relative roughness values from these
evaluations, yielded a relative roughness ϵ/D =0.0025 or a pipe roughness
ϵ = .000038 ft. This roughness value lies between that of commercial
steel and drawn tubing (ϵ = .00015 and ϵ = .000005 respectively). The
model vent pipe material is drawn stainless steel.

This relative roughness value was used to model the vent restrictions
employed for subsequent evaluations. The vent restriction was modeled by
first establishing the Reynolds number at which the test would be run.
This would simply be the vent pipe velocity of the test ($\dot{Q}$/A) times the
model vent pipe diameter (D) divided by the kinematic viscosity of the
fluid being vented (e.g. air). The friction factor, 4f,would then be es-
tablished by finding the intersection of the relative roughness curve for

.2 VENT PIPE OF LENGTH L

PRESSURE
TRANSDUCER

.1
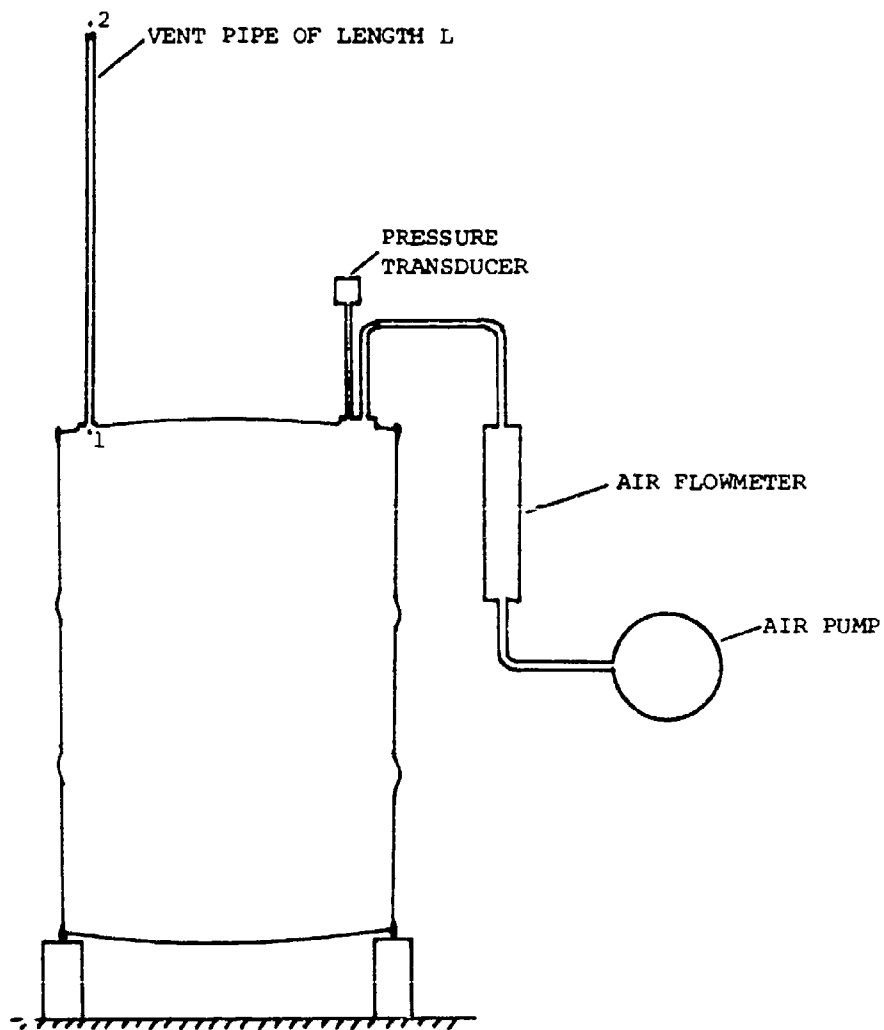
AIR FLOWMETER

AIR PUMP

FIGURE A1 - SCHEMATIC OF EXPERIMENTAL TEST SETUP
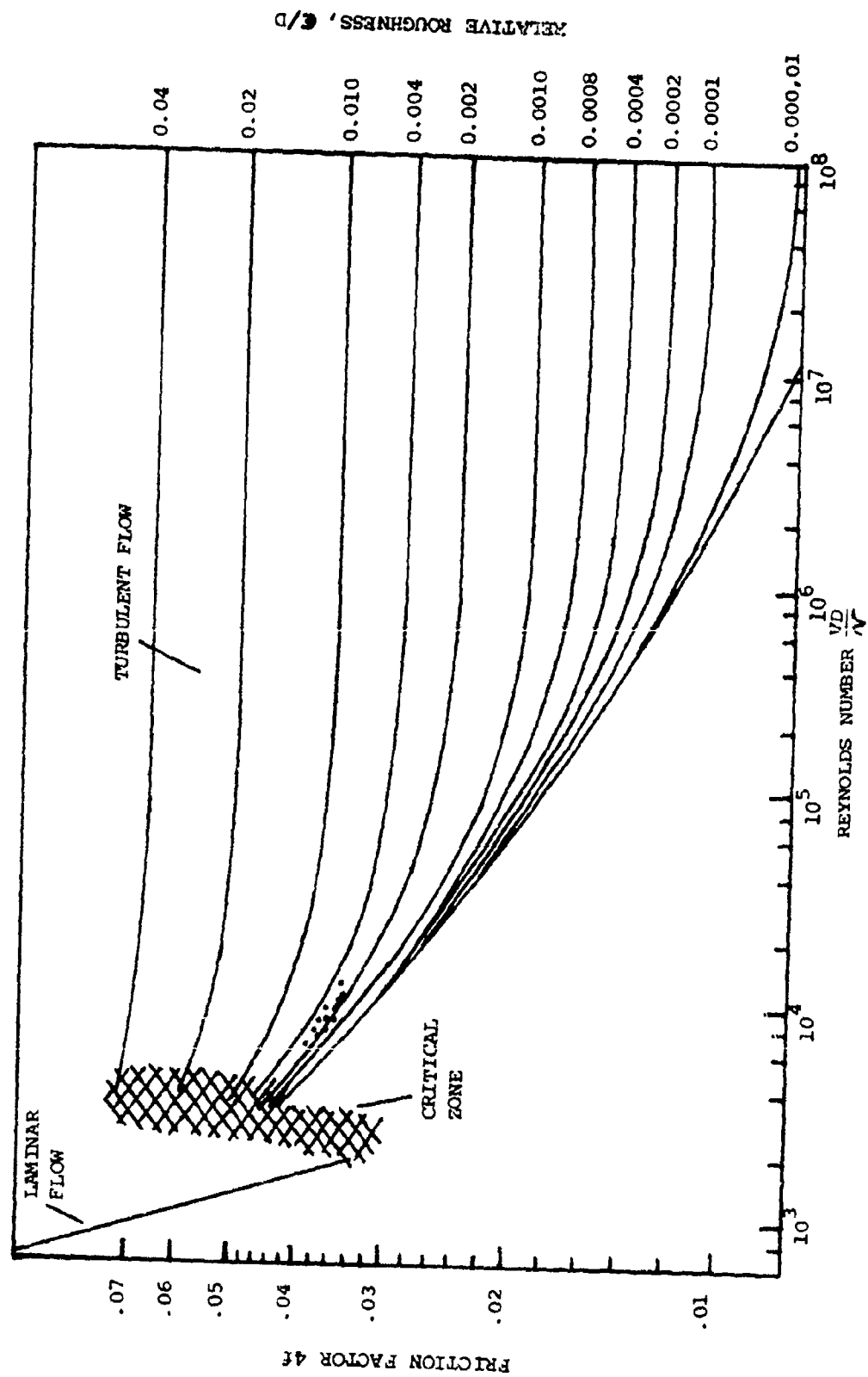   FOR VENT PIPE ROUGHNESS DETERMINATIONS

67

FIGURE A2 - RESULTS OF MODEL VENT PIPE ROUGHNESS DETERMINATIONS

68

the pipe and the Reynolds number at which the test was run on a Moody diagram. Knowing the friction factor 4f and the vent pipe diameter D, the desired value of 4f L/D could now be modeled (for this particular Reynolds number) by cutting the model vent pipe to the appropriate length, L.

For example:

To model

$\dot{Q}/A$ = 100 ft/sec and 4f L/D = 20 with D = .0155 ft compute,

Re = $VD/_{\mathcal{N}}$ = 100 x .0155/.000162 = 9568, from Moody diagram for

Re = 9568 and ϵ/D = .0025 we get

4f = .035 and then L = 8.85 ft.

Since the flow state for the evaluations was not fully turbulent (4f not constant) and new lengths of pipe were not employed for each loading rate examined, the actual vent restriction 4f L/D was arrived at using the pipe relative roughness to account for 4f not being constant with changing loading rates. Consider the above example, but with the vent pipe velocity $\dot{Q}/A$ = 50 ft/sec. For this case the Reynolds number Re = 4784 and the friction factor 4f = .041, resulting in 4f L/D = 22.8. This correction is reflected in the (actual) 4f L/D values given in Tables 2, 3 and 4. Additionally, in the design of the transfer experimental parameters, care had to be taken so that a combination of 4f L/D (pipe length and diameter) and transfer rate $\dot{Q}/A$ (pumping rate and vent area) were not employed such that Mach 1 was attained in the vent.

APPENDIX B

MOIRE' METHOD FOR MEASURING PLATE DEFLECTIONS

Since 95% of the tank volume change by pressure occurred from the
tank top and bottom deflections and since the change in tank volume with
pressure (bulk modulus) is an important parameter for overfill, it was
felt that a backup method (in addition to the linear potentiometer) for
measuring the tank top and bottom deflections would be advantageous. To
accomplish this, the Moire' Contour Sum-Contour Difference Method was em-
ployed to measure the plate deflections in the tank top and bottom.

Briefly, the Moire' method employed here consisted of the observation
of contour-like patterns created by the mode interference of a grid with
its shadow cast onto a surface (the tank top). A photograph of the pattern
is made and stored and the tank top is then allowed to deform by increasing
the internal tank pressure. A second exposure of the tank top is then made
over the first exposure by double exposing the film. The result of this
process is the development of Moire' interference fringes which depict
contour differences on the surface photographed. The contour elevations
can be calculated knowing the distances of the projected grid and camera
from the surface, the angles they form with the surface in question, and
the grid spacings.

Figure B-1 shows the deflections measured on the tank top and bottom
employing the Moire' method to arrive at the change in tank volume for
a 25 psig internal pressure. These measurements were made statically by
projecting the Moire' grid on the tank, taking an exposure of the pattern,
pressurizing the tank to 25 psig and taking a second exposure. The resulting
photograph recorded the Moire' fringes thus produced, which when converted
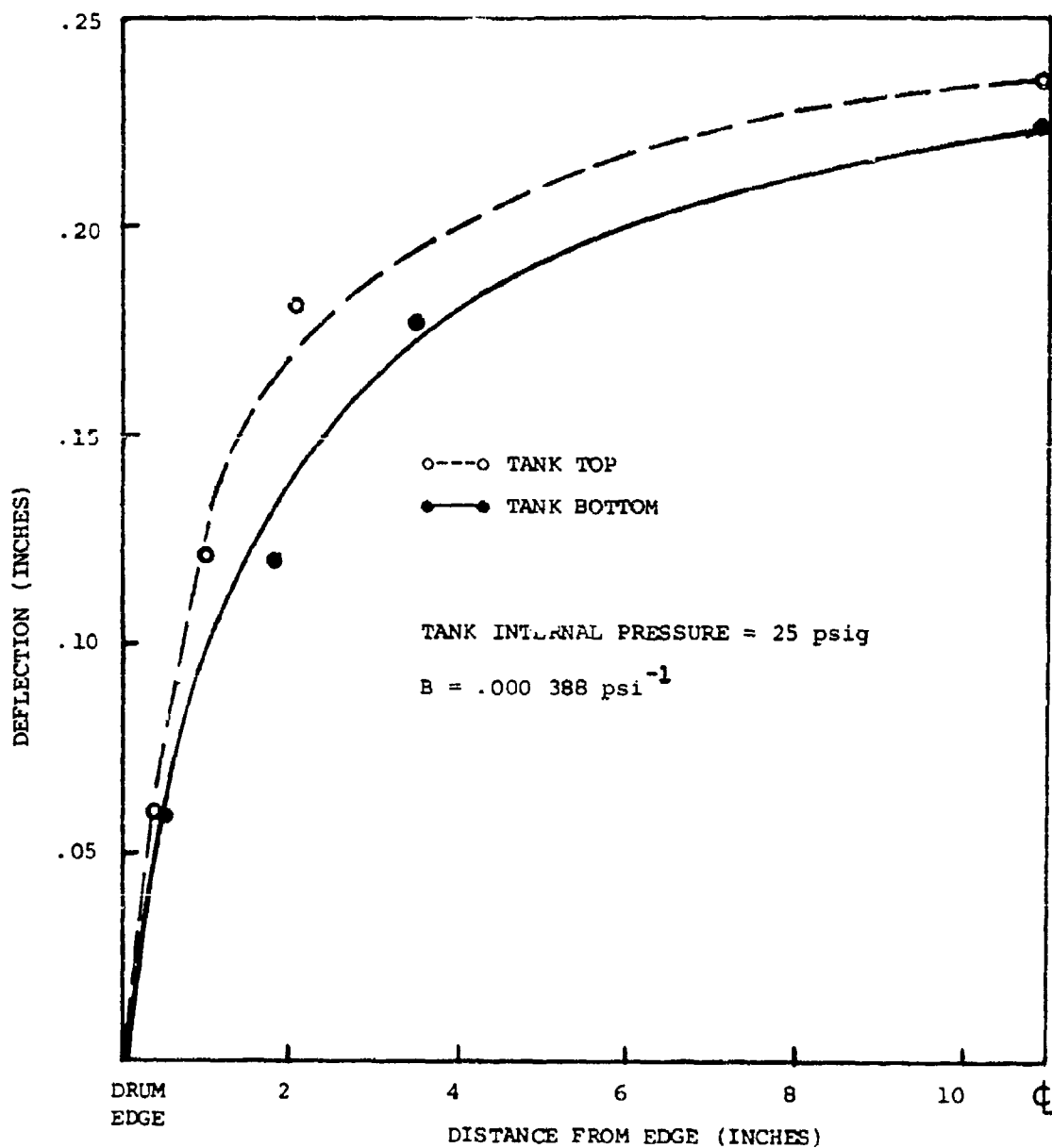
71

FIGURE B1 - RESULTS OF STATIC TANK BULK MODULUS DETERMINATION
USING MOIRÉ METHOD

to deflections produced the deflection pattern shown in Figure B-1. A micrometer was used to measure the deflection of the center of the tank top and bottom plate to give an additional data point for this static tank calibration.

To arrive at the tank bulk modulus $B = \Delta V / \Delta p \, V_T$, additional information from the tank strain channels (hoop strain and the longitudinal cylindrical extension strains) was employed in conjunction with the Moiré results, to arrive at the total tank volume change. The results of this static bulk modulus determination can be found in Table B-1.

The value for B thus determined was then used in the analytical expression for a blocked vent to predict the blocked vent pressure time history. Additionally, the Moiré method was employed during the actual experimental overfill evaluations to get the time dependent volume changes during overfill. This was accomplished by exposing motion picture film of the grid on the tank top before testing, rewinding the exposed film, then running the test and re-exposing the same film during the test. The result was a time dependent contour map which could be equated to a time dependent volume change and bulk modulus. The change in bulk modulus as a function of time (pressure) was less than 20% and the assumption of a constant value for the bulk modulus considered valid for comparative purposes with the analytical model (assumes constant B).

TABLE B-1

Tank Pressure $= 25$ psig	$V_{Tank} = 13{,}281 \text{ in}^3$
$\Delta V_{Tank\ Top} = 69.0 \text{ in}^3$	$\Delta V_{Long} = 1 \text{ in}^3$
$\Delta V_{Tank\ Bottom} = 57.0 \text{ in}^3$	$\Delta V_{Hoop} = 2 \text{ in}^3$

$$B = \frac{\Delta V}{V_T \Delta p} = \frac{129}{13{,}281 \times 25} = .000388 \text{ psi}^{-1}$$

73